Abstract

Miller, Scott Franklin. Wire Electro-Discharge Machining of Advanced Engineering Materials. (Under the direction of Dr. Albert Shih)

The goal of this research was to create models and guidelines for Wire Electrical Discharge Machining (WEDM) of new advanced engineering materials and for truing of metal bond diamond grinding wheels. The development of new advanced engineering materials and the need to meet demand for precise and flexible prototype and low-volume production of components has made WEDM an important manufacturing process. One goal of this research is to investigate the effect of spark on-time duration and spark on-time ratio, two critical WEDM process parameters, on truing of metal bond diamond grinding wheels and machining of three types of new advanced engineering materials; porous metal foams, sintered Nd-Fe-B magnets, and carbon-carbon composite fuel cell bipolar plates. An envelope of feasible process parameters for material removal rate is developed for each material, according to machine, tooling, and physical limitations. This envelope is then applied to cut sections of carbon-carbon bipolar plate and sintered Nd-Fe-B magnet to minimum thickness. Effect of process parameters on limit of thickness of the sintered Nd-Fe-B magnet is discussed. The surfaces machined by WEDM were qualitatively studied using Scanning Electron Microscopy to observe surface features and characteristics. Experiments were conducted to measure temperatures generated during the EDM process using infrared spectrometry on three different materials; 1. metal bond diamond grinding wheel, 2. WC-Co, and 3. copper.

Wire Electro-Discharge Machining of Advanced Engineering Materials

by

Scott Franklin Miller

A thesis submitted to the Graduate Faculty of
North Carolina State University
in partial fulfillment of the
requirements for the Degree of
Master of Science

Department of Mechanical and Aerospace Engineering

Raleigh

2003

APPROVED BY:

_____ _____

_____
Chair of Advisory Committee

Biography

Scott Miller was born in Boone, a small town in the mountains of western North Carolina. He was the first of three children in the Miller family. During Scott's childhood his parents supported academics, sports, and activity, in that order. In elementary school and high school Scott enjoyed playing sports and hanging out with his friends. Football and baseball were the sports of choice. After high school he was unsure of his future plans; so he decided to attend Appalachian State University to continue his education. During his first two years of college he discovered his inclination to math and science. In order to focus on and combine these subjects, he decided to pursue a degree in Engineering. In the Fall semester of 1999, he transferred to North Carolina State University in Raleigh, NC. From his first class in Engineering, he was sure that he had made the correct decision. After five semesters and a semester of Cooperative Education, he graduated Summa Cum Laude with a Bachelor of Science in Mechanical Engineering in the spring of 2002. During his undergraduate studies at North Carolina State University Dr. Albert Shih recruited him for graduate studies. Under the guidance of Dr. Albert Shih, Scott has spent the last two semesters working toward obtaining a Master of Science Degree in Mechanical Engineering. He conducted his research at NC State University and Oak Ridge National Lab. He will be graduating in May and beginning work toward his Ph.D.

Acknowledgements

To Dr. Albert Shih, I am glad you convinced me to come to graduate school; I value the things I learned about myself as much as the technical knowledge gained. Your kindness, patience, and laughter made the experience enjoyable. To my committee members, Dr. John Strenkowski and Dr. Ron Scattergood, I appreciate the contribution of your time and efforts.

Thanks to Oak Ridge National Laboratory especially the High Temperature Materials Laboratory for facilitating me during my SEM investigations. Special thanks must be given to Sam McSpadden and Dorothy Coffey for their assistance and preparation before each of my visits.

The authors acknowledge Magnequench and Dr. B. M. Ma for the sintered Nd-Fe-B permanent magnets, Porvair PLC and Dr. K. Butcher for the metal foam and carbon-carbon bipolar plate, and Cummins Inc. and D. J. Gust for the diamond grinding wheels.

Table of Contents

List of Tables

Chapter 2

Chapter 3

Chapter 5

List of Figures

Chapter 1

Chapter 2

Chapter 3

Chapter 4

Chapter 5

Chapter 1. Introduction

The development of new advanced engineering materials and the need to meet demand for precise and flexible prototype and low-volume production of components has made wire electrical discharge machining (WEDM) an important manufacturing process. The WEDM

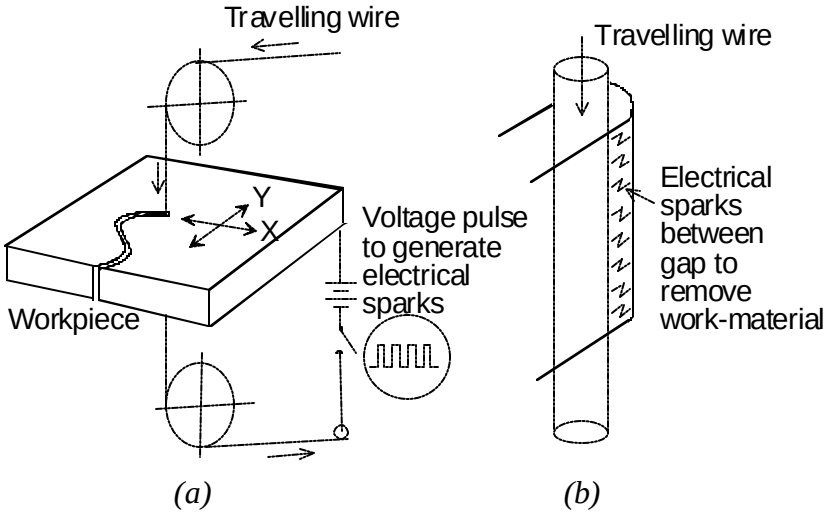

Figure 1.1: The wire EDM process, (a) conventional 2D wire EDM operation, (b) enlarged view of the wire and workpiece

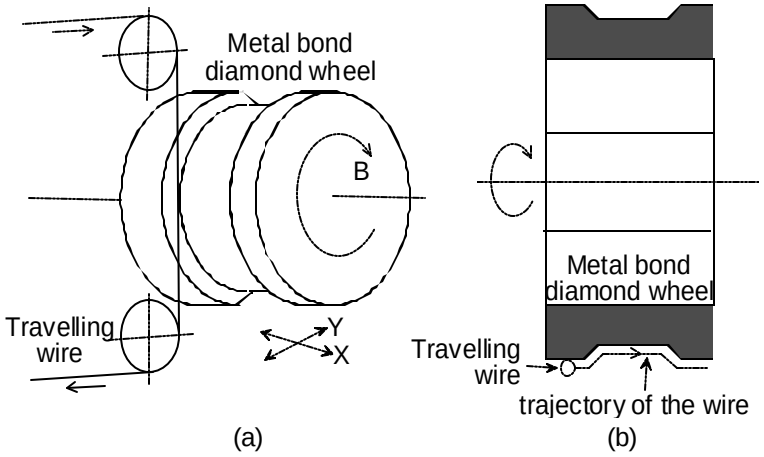

Figure 1.2: Wire EDM of metal bond diamond wheel, (a) configuration of the operation, (b) top view of the trajectory of the wire

process, as shown in Figure 1.1(a), generates the desired shape by using electrical sparks between a thin, traveling brass wire electrode, ranging from 0.02 to 0.40 mm in diameter, and workpiece to erode a path in the workpiece material. Figure 1.1(b) shows continuous electrical sparks being generated between the wire and workpiece for material removal. By using computer numerical control, the thin wire is guided in X and Y directions to cut a precise shape from the workpiece. The cutting force generated in WEDM is small, which makes it suitable for manufacturing miniature features and micro-mechanical components. This process can also be used to machine cylindrical parts and true metal bond diamond grinding wheels, by adding a rotary spindle to the WEDM machine, as Figure 1.2 shows.

The selection of proper process parameters for new WEDM applications, such as machining advanced engineering materials, micro-fabrication, truing of diamond grinding wheels, etc, is not readily available. Process parameter selection has a significant effect on WEDM efficiency and limitation. For a commercial WEDM machine, the manufacturer usually provides a database of setup process parameters for commonly used work and electrode materials under typical operating conditions. Such a database does not include the growing amount of advanced engineering materials or WEDM applications. One of the goals of this research is to investigate the effect of spark on-time duration and spark on-time ratio, two critical WEDM process parameters, on truing of metal bond diamond grinding wheels and machining of three types of new advanced engineering materials: porous metal foams, sintered Nd-Fe-B magnets, and carbon-carbon composite fuel cell bipolar plates. An envelope of material removal rate for selection of process parameters is generated for each material. This envelope is applied to enable the machining of thin sections of carbon-carbon bipolar plate and sintered Nd-Fe-B magnet. Based on experimental results and observations,

models and guidelines for WEDM of new engineering materials and for truing of metal bond diamond grinding wheels are developed.

The removal of material depends largely on thermal principle; the EDM machine supplies the system with electrical energy, which is mainly converted into thermal energy in the discharge channel during the spark discharge. The thermal energy melts workpiece material during the process. To acquire more insight into the processes of EDM, including the phase transitions of the machined material, it is important to know the temperature of the machined material. Another goal of this research is to measure temperature during WEDM machining using infrared spectrometry. Measurements are taken on a variety of materials, including WC-Co, copper, and metal bond diamond grinding wheels.

A description of the WEDM process is in Chapter 1. Chapter 2 provides WEDM basic principles, experimental setup, and background for the material removal rate study, which focuses on machining new advanced engineering materials. Chapter 3 gives the results of the material removal rate study and cutting of thin sections of sintered Nd-Fe-B magnets. SEM investigation of surface finish is carried out in Chapter 4. Chapter 5 presents the research on spark temperature measurements by using near infrared spectrometry. And the final discussion is presented in Chapter 6.

Chapter 2. Experimental Setup

Since new WEDM applications, such as machining of new advanced engineering materials, micro-fabrication, truing of diamond grinding wheels, are not a traditional process, the selection of proper process parameters is not readily available. Material removal rate (*MRR)* depends heavily on process parameter selection. The goal of this study is to investigate the effect of spark on-time duration and spark on-time ratio, two critical WEDM process parameters, on truing of metal bond diamond grinding wheels and machining of three types of new advanced engineering materials; porous metal foams, sintered Nd-Fe-B magnets, and carbon-carbon composite fuel cell bipolar plates. For each of these materials, an envelope of *MRR* is generated based on selection of process parameters. This envelope is applied to cut thin sections of carbon-carbon bipolar plate. Effect of process parameters on limit of thickness of the sintered Nd-Fe-B magnet is discussed. A model for WEDM of thin sections of sintered Nd-Fe-B magnets is developed.

Some papers discussing EDM performance concern volumetric material removal of materials such as SiC/Al, PCD blanks, and advanced ceramics, while varying certain parameters [Hocheng et al.,1997; Kozak et al., 1994; Lok et al., 1997].

2.1. Basic Principles of Electrical Discharge Machining

The following figure and description represents what is known and what is theorized behind the generation of spark erosion in the EDM process. Several theories have been presented over the years regarding how EDM works. But most of the evidence supports the thermo-electric model. The nine illustrations in Figure 2.1 show what is believed to happen during the generation of a single spark in the EDM process. Graphs near the bottom of each

illustration show how the voltage and current relatively vary from step to step. In all of the diagrams, the wire electrode (anode) is the upper dark material of positive charge and the workpiece is the lower serrated part of negative charged. The dielectric fluid in the machining gap separates these two surfaces, and serves as an insulator to keep electrical charge from flowing from one surface to another [Rajurkar, 2001].

Figure 2.1(a) shows what happens with the charged electrode is first brought near the workpiece. As the potential difference increases between the surfaces, the dielectric fluid breaks down and becomes ionic (electrical conductive). The electrical field is strongest at the point where the distance between the surfaces is minimal; thus the spark will occur at this location. Note the graph in the illustration shows potential (voltage) has increased, but no current is flowing because of the presence of the dielectric fluid.

Next as shown in Figure 2.1(b), the number of ionic particles increases, making the insulating properties of the dielectric fluid begin to fail along a narrow channel at the high point. Voltage reaches its peak, but current is still not flowing.

Figure 2.1(c) shows that a current is established, causing the voltage to decrease. Figure 2.1(d) shows the voltage is continuing to drop as current continues to rise. The heat builds up rapidly, causing some of the fluid, workpiece, and electrode to vaporize. A discharge channel now begins to form between the electrode and workpiece.

Figure 2.1(e) depicts a vapor bubble trying to expand outward, but a rush of ions towards the discharge channel limits its expansion. The intense electro-magnetic field that has built up in the channel attracts these ions. The current continues to rise as the voltage continues to drop.

Figure 2.1(f) is during the end of the time when the voltage is on. Here the current and voltage have stabilized. The heat and pressure inside the bubble have reached maximum

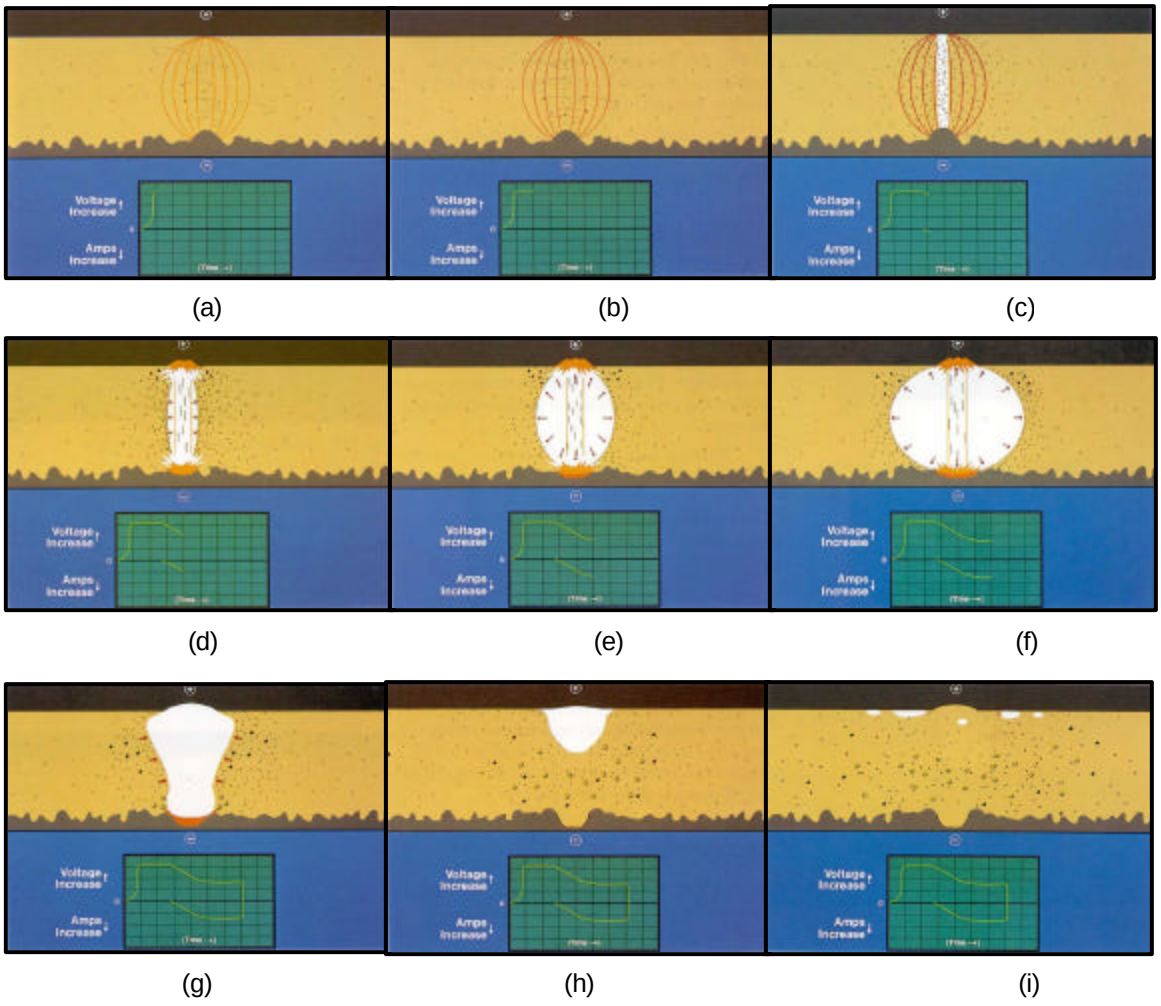

Fig. 2.1: Evolution of a single spark in the EDM process [Rajurkar, 2001].

values and some metal is being removed. The metal directly under the discharge column is in the molten state, but is held in place by the pressure of the vapor bubble.

Figures 2.1(g) 2.1(h), and 2.1(i) show what happens during the time when no voltage is applied. Both voltage and current go to zero, which causes the temperature and pressure to rapidly decrease in the vapor bubble causing it to collapse. This collapsing bubble allows the molten material to be expelled from the surface of the workpiece. Fresh dielectric fluid

rushes in, flushing the debris away and quenching the surface of the workpiece. Unexpelled molten metal solidifies back to the surface to form what is known as the recast layer. This complete process of voltage on and off time comprises the EDM spark cycle.

2.2. Description and Background of Materials

2.2.1. WEDM Machine

The WEDM experiments are conducted on a Brother HS-5100 WEDM. Results in this study are machine dependent. However, the results obtained in this research can be summarized into guidelines and applied or calibrated to different kinds of WEDM machines. A commonly used copper wire of 0.25 mm nominal diameter is used for wire electrode.

2.2.2 Work Materials

Six work materials include two metal foams, two metal bond diamond grinding wheels, one sintered Nd-Fe-B magnet, and one carbon-carbon bipolar plate. A description of the new advanced engineering materials researched follows:

1. *Metal Bond Diamond Grinding Wheels*: The advancement of engineering ceramics is hindered by high manufacturing cost, particularly in precision grinding to generate the desired form geometry. This technical challenge is further narrowed down to generate the precise form on diamond grinding wheels. Diamond, the hardest material, is difficult to form using a diamond tool.

The wire EDM process can be used to create an intricate shape on a rotating metal bond diamond wheel for precision form grinding of ceramics and other difficult-to-machine materials [Rhoney, et al., 2002]. The concept studied in this research is using the wire EDM to machine or true a rotating metal bond diamond wheel, as shown in Figure 1.2, to generate the precise form. By adjusting the process parameters, high *MRR*, higher than 2D EDM cutting, can be achieved. This study also identifies critical process parameters and boundaries that limit *MRR*.

Much research has been conducted on the EDM over the past two decades. However, much of the work has been on developing better power sources, discharge patterns, and improving gap conditions. One of the first papers that discussed EDM truing was by Suzuki et al. [1987]. This paper considers both wire and electrode EDM of metal bonded wheels. It discusses the problems associated with traditional truing of the hard metal bonded wheels.

Two metal bond diamond grinding wheels were studied. One has the 320 ANSI mesh size diamond (average size of 54 μm). This wheel was manufactured by Norton/Saint-Gobain with tradename of Scepter. The other is a bronze bond diamond wheel (Inland MD1200N50M-1/4) with very fine, 1200 ANSI mesh size diamond (average size of 6 μm).

2. *Porous Metal Foams*: Metal foam materials have great potential for the fuel cell and lightweight structural material for aerospace and automotive applications. EDM is particularly suitable for machining metal foam due to the low cutting force to avoid the damage on the ligaments and thin walls in metal foams. This research studies effects of EDM process parameters on *MRR* of porous metal foam.

Table 2.1: Material comparison

Material	Fe-Cr-Al	316 Stainless Steel
Density (kg/m^3)	7150	7980
Electrical resistivity (ohm-mm)	0.0014	0.00078
Heat capacity (J/g-°C)	0.46	0.49
Thermal conductivity (W/m-k)	16	16.3
Melting temperature (°C)	1500	1400
Yield strength (MPa)	550	290
Ultimate tensile strength (MPa)	750	580

Table 2.1 gives a material comparison of the two types of porous metal used in this research. One material is the Fe-Cr-Al alloy, which is a high temperature oxidation resistance material that can withstand operation temperature in excess of 1200 C. The other material is 316 stainless steel porous metal. The foam structure, as shown in pictures from a scanning electron microscope in Figure 2.2, consists of ligaments making up a network of interconnected, dodecahedral-shaped cells. The cells are oriented randomly. The individual ligaments are hollow with a triangular-shaped shaft, which is a result of the applied manufacturing technique. The metal foams are produced using open cell polyurethane foam as a template [Ashby et al., 2000; Banhart, 2001]. The metal powder slurry is coated to the polyurethane foam and fired in a kiln. The polyurethane foam is burned out during the process, leaving the triangular-shaped hollow shaft inside each of the ligaments.

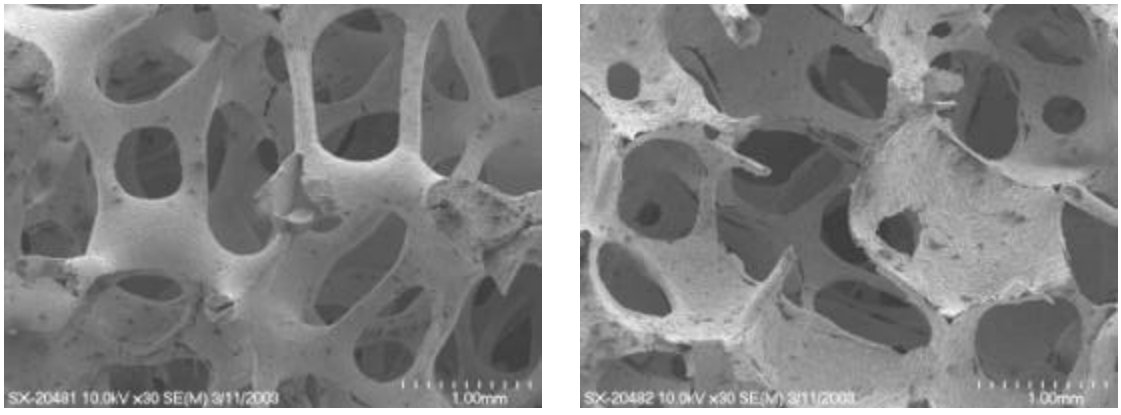

(a) *(b)*

Figure 2.2: (a) Porous 316 stainless steel foam (b) Porous Fe-Cr-Al foam

3. *Sintered Nd-Fe-B Permanent Magnetic Materials*: The needs for energy-efficiency and miniaturization of mechanical devices have created applications of rare-earth permanent magnets as opposed to traditional ferrite. The sintered Nd-Fe-B magnet has the combined cost and performance benefits. This material is very brittle. The magnet is Neomag 34KC2, provided by Magnequench. The nanocrystalline Nd-Fe-B powder is sintered by the hot-isostatic press and then magnetized to become the permanent magnet. This research investigates effects of EDM process parameters on *MRR*, as well as wire EDM of miniature features of Nd-Fe-B permanent magnets for miniature motor, generator, and actuator applications. In this study an additional set of tests was conducted to evaluate variation in thickness due to EDM process parameters when machining miniature features.
4. *Carbon-Carbon Bipolar Plates:* Proton exchange membrane fuel cell development challenges include reducing weight, cost, and volume of the fuel cell stack. A key component of the fuel cell is the bipolar plate that separates cells in the stack and provides channels for gas flow. The requirements for bipolar plates include cost of material and processing. The carbon-carbon bipolar plate, provided by Porvair LLC, uses slurry molded carbon fibers, about 0.4 mm long and 0.01 mm in diameter, which is sealed with chemically vapor-infiltrated carbon [Besmann et al., 2000]. The material has an electrical conductivity of 0.4 Ocm^2 at 1.15 A/cm^2 and 0.9 Ocm^2 at 0.05 A/cm^2 current density. A plate of 2.3 mm thickness is used in this study. An additional set of tests was conducted to illustrate the application of region of feasible process parameters to enable the production of features with minimum thickness.

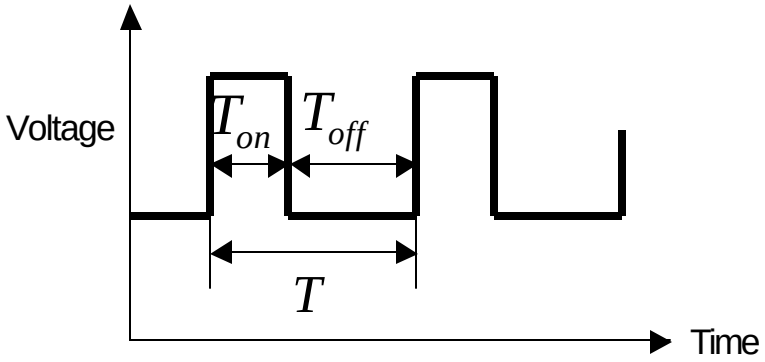

Figure 2.3: Diagram of voltage cycle in EDM

2.3. Setup of Material Removal Rate Study

When performing the removal rate study WEDM certain procedures must be followed in order to insure maximum *MRR*. The description of process parameters and experimental procedure follow.

2.3.1. Process Parameters for Material Removal Rate Study

Since WEDM of the materials in this study is not a traditional EDM process, predetermined EDM parameters are not established. Through an understanding of how the parameters interact and trial and error the parameters are adjusted to perform this research. A discussion of the significant process parameters follows:

The two main process parameters investigated in this study are spark cycle and spark on-time. Figure 2.3 shows the ideal waveform of voltage between the workpiece and electrode versus time during EDM. As shown in Figure 2.3, the spark cycle, T, is the period of the spark, including both on time and off time. EDM uses a DC power supply and capacitor like energy storage bank to create the discharge. During the off time, T_{off}, the capacitors are charged up and melted material is flushed from the gap between the wire

electrode and workpiece. Then the circuit is completed, the spark is discharged, and the energy is delivered during the on time, T_{on}, which is the spark on-time. This total time for charging and discharging is the spark cycle. This research studies the effect of T_{on} and T_{on}/T on EDM *MRR*.

The gap voltage is the nominal voltage in the gap between the wire and workpiece. Thus, increasing distance between the wire and workpiece means increasing gap voltage, and vise versa. Increasing gap voltage also usually means decreasing cutting speed. The WEDM training manual compares gap voltage to feed of workpiece of a band saw.

Wire feed rate is traverse velocity of the wire as it moves through the workpiece. It determines how fast you cut the workpiece. It is important to note that this is not a constant speed, but it can be thought of as maximum possible speed. The machine reads the actual gap voltage, and automatically increases or decreases feed rate to maintain constant gap voltage.

2.3.2. Workpiece Setup

As shown in Figure 2.4, in typical WEDM the workpiece is fixed to a worktable, which serves as the electrical ground, inside the EDM machine to complete the circuit. In order to determine orientation of the workpiece relative to wire, an edge find command is executed. The wire moves in slowly until it detects the electrical ground of the workpiece. The wire is then backed away from the edge about 2.5 mm in order to allow sufficient space for the machine to automatically rethread the wire in the event of wire breakage. This is the starting point from which machining will begin, as shown in Figure 2.5. Finally, the

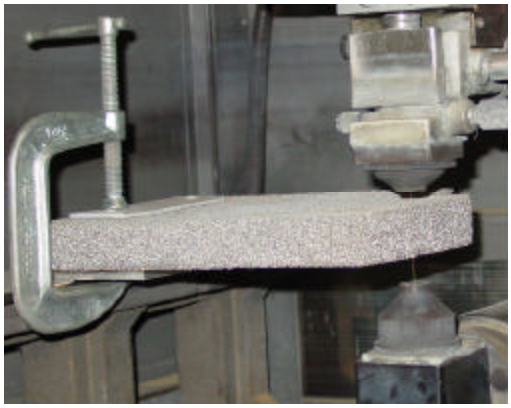

Figure 2.4: Fixed workpiece

Figure 2.5: Starting position of cut

workpiece in EDM is submerged in a dielectric fluid for improved flushing and thermal control.

The preparation for the metal bond diamond grinding wheels is different from the above setup in the following respects. The grinding wheel is attached to a hub. The wheel/hub assembly is attached to the shaft of a rotary spindle, which is bolted to the worktable in the EDM machine. Only the water jets provide the dielectric fluid; the fluid does not submerge the grinding wheel. Flushing is not an issue, since the wire is only working on the surface, and is not buried within the material.

2.4. Experimental Procedure

Experiments are conducted during machining a straight path into the workpiece. During the experiments five T_{on} at 18, 14, 10, 6, and 4 μs are selected. It should be noted that the setting of 4 μs generates energy density that is too small, at any spark cycle, T, to cut the sintered Nd-Fe-B magnet or the metal bond diamond grinding wheels. At each T_{on}, the ratio of T_{on}/T is gradually increased until wire breakage and decreased until wire short occurs. All other process parameters are held constant during the experiments, excluding the wire feed

rate. The EDM machine automatically varies the wire feed rate, or cutting speed, in an attempt to maintain the target gap voltage. During the *MRR* experiments the wire feed rate is averaged over the entire cutting time. These averages are the collected data.

The range for spark cycle (T) is from 10–1000 µs, and for spark on-time is from 2–18 µs. These values correspond to the machine limits for the Brother HS-5100 WEDM. It should be noted that the setting of 2 µs is a special low energy setting not used in typical EDM machining. Wire feed rate is set at 15 mm/s, wire tension at 0.15 N, and gap voltage between wire electrode and workpiece is set at 35 V.

2.5. Procedure for Cutting Thin Sections

A growing WEDM application regards fabrication of miniature components. An application of the envelope of process parameters is cutting thin sections. Process parameters used in cutting carbon-carbon bipolar plate thin sections are determined from the acquired envelope for the carbon-carbon bipolar plate. The process parameter settings for maximum energy density and minimum energy density are selected. The three selections of spark on-time used for cutting thin sections of sintered Nd-Fe-B magnet material are 18, 10, and 2 µs, which are chosen based on spark on-time available range.

In each cut of the carbon-carbon bipolar plate length of cut is 24.0 mm. In each cut of sintered Nd-Fe-B magnet material height is 1.5 mm and the machine is stopped after a length of 3 mm of cutting. In each experiment made with a certain set of process parameters, the cut of specified dimensions is made with the third dimension decreasing with each cut, until the thin section can no longer sustain the thickness of the cut attempted.

Chapter 3. Results of Material Removal Rate Study and Cutting Thin Sections

There are machine, tooling, and physical limitations that constrain the material removal process in WEDM. An envelope of feasible T_{on} and T_{on}/T process parameters can be generated on the chart of material removal rate, (*MRR*), vs. T_{on}/T to characterize the WEDM process for a particular material. The limitations, *MRR* envelope, and results of the *MRR* study are discussed in Chapter 3.

3.1. Envelope of Material Removal Rate

Figure 3.1 shows a sample graph of the envelope of process parameters for traditional WEDM application. The *MRR* for each material follow this general format. In the graph the X-axis represents T_{on}/T (%), or percentage on-time of the spark. The Y-axis represents rate of performance for the WEDM machine. The actual units vary depending on the type of machining performed. For non-rotary applications (porous metal, permanent magnet,

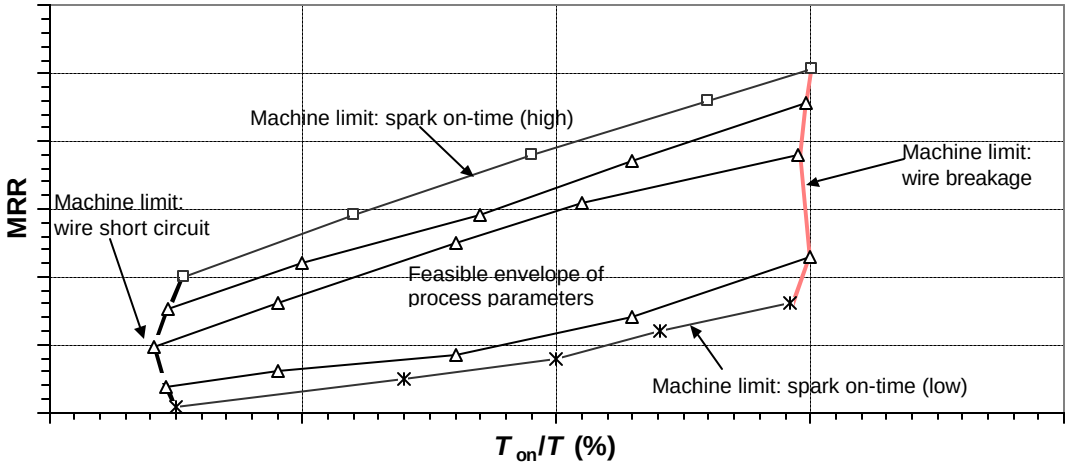

Figure 3.1: Typical envelope of the WEDM process

carbon-carbon bipolar plate, steel plate), the Y-axis represents wire feed rate, or cutting speed of the wire through the workpiece in units of mm/min. For rotary applications (diamond grinding wheel), the Y-axis represents *MRR* in units of mm^3/min.

The 5 spark on-time settings, T_{on}, selected (18, 14, 10, 6, 4 μs) are represented in the Figure 3.1 as series with specified markers. The machine upper and lower limits for T_{on} are 18 and 4 μs, respectively. For every material studied with the exception of the carbon-carbon bipolar plate, the major machine limits of wire breakage and wire short circuit existed. When the spark on-time ratio, T_{on}/T, reaches an upper limit, the energy density is high, and occurrence of electrical spark becomes frequent. This results in the electrical sparks eroding the wire to the point of wire breakage during cutting, which is represented by the thick solid line in Figure 3.1. When T_{on}/T approaches the lower limit, the energy density is low, and occurrence of electrical spark becomes rare, increasing the risk of the wire electrode touching the workpiece. The event of wire touching workpiece shorts the electrical circuit, and causes cutting to stop due to the wire short circuit alarm, which is represented in Figure 3.1 by a thick broken boundary. It should be noted that these boundaries are not exact. These boundaries merely indicate high probability that the indicated machine limit will be reached.

In each graph, excluding the graph for the carbon-carbon bipolar plate, thin lines without markers represent regression modeling. In this study regression modeling is performed directly on the source data in the data analysis package of Microsoft Excel. The purpose of regression modeling is to find a relationship among certain factors in an analysis. In this study, the factors of significance are EDM *MRR*, T_{on}/T, and duration of spark

cycle, *T*. The form of the regression model for *MRR* is:

$$MRR = a \cdot \left(\frac{T_{on}}{T} \right)^{b} \cdot (T)^{c} \tag{1}$$

The regression analysis determines variables *a*, *b*, and *c* in the equation.

3.2. Results of Material Removal Rate Study

MRR is used to measure the efficiency of a process. The effects of T_{on} and T_{on}/T are key factors regarding *MRR*. The results of the *MRR* study follow. An envelope of process parameters is presented for each material in the study along with discussion.

3.2.1. Metal Foams

Figure 3.2 shows the envelope of process parameters for 316 stainless steel foam, Fe-Cr-Al foam, and the carbon steel plate, with the same effective thickness as the foams. As the graph illustrates, under similar cutting condition, higher *MRR* is possible with the metal foams. This is due to the better flushing condition with the porous metals. The 316 stainless steel foam has a higher *MRR* than the Fe-Cr-Al foam. This can be predicted from the material properties of electrical resistivity and melting temperature, since EDM uses electrical sparks to melt the material it removes. Fe-Cr-Al and 316 stainless steel have electrical resistivities of 0.0014 and 0.00078 ohm-mm, respectively, and melting temperatures of 1500 and 1400^{o}C, respectively. The maximum wire feed rates for Fe-Cr-Al and 316 stainless steel foam is 45.7 and 50.8 mm/min, respectively. The steel sheet metal

proved to be most difficult to cut, with a maximum feed rate of only 18.8 mm/min. Letters in the metal foam graphs signify process parameters to be investigated in the SEM study in Chapter 4.

It should be noted that regression analysis, shown in thin lines in the *MRR* graphs is not perfect. For most of the data regression analysis closely modeled the *MRR*. However, regression analysis is not perfect, and regression lines did stray from the experimental curve in some graphs. The regression model for 316 stainless steel appears to be the most inaccurate of the regression modeling.

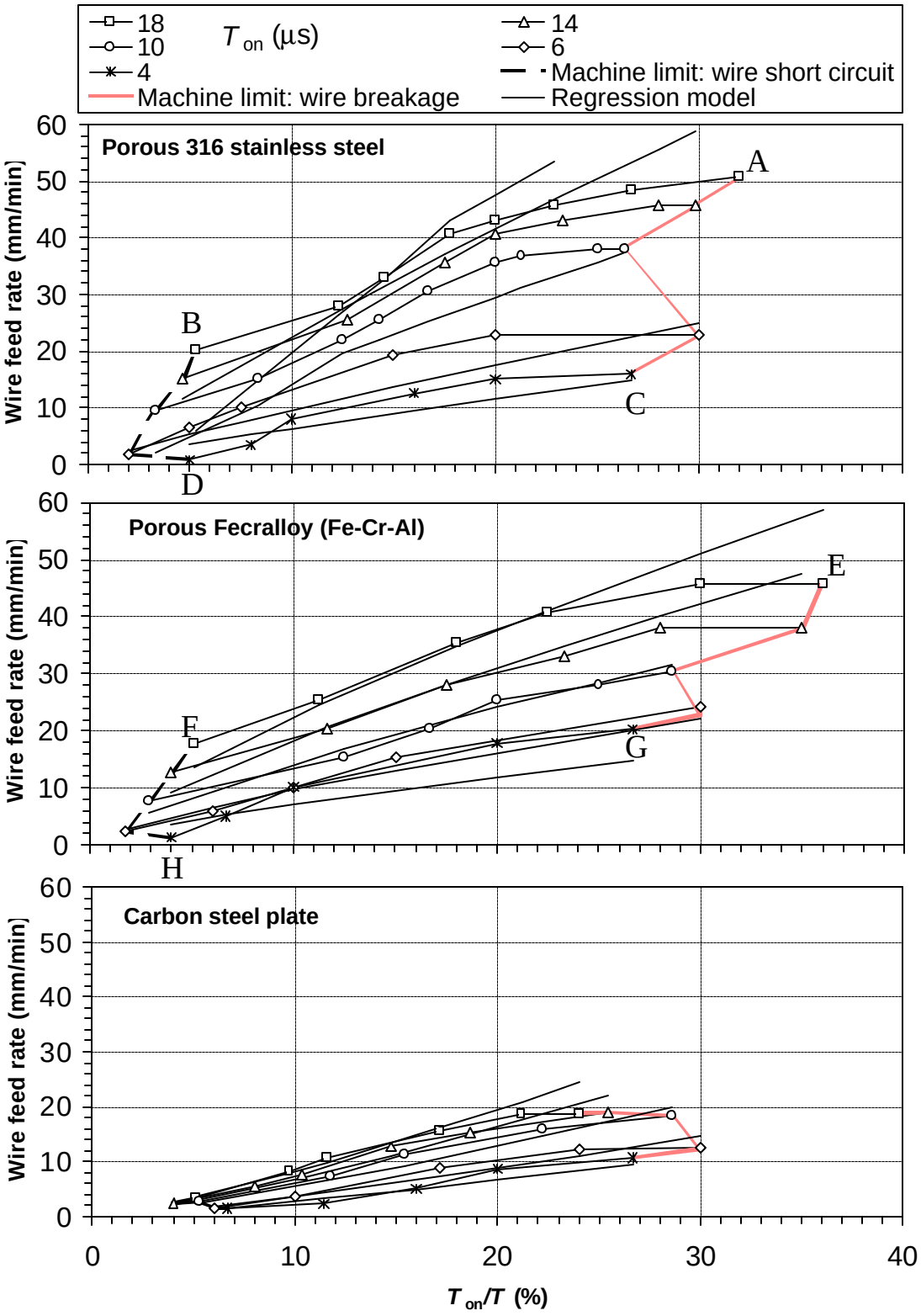

Figure 3.2: Material removal rate graphs for porous metal foams and steel plate

3.2.2. Metal Bond Diamond Grinding Wheels

As mentioned earlier, the machine performance measured is volumetric *MRR* for metal bond diamond grinding wheels. The mathematical formula to calculate the material removal rate for cylindrical wire EDM has been derived by Qu et al. [2002a]. The straight truing configuration, as shown in Figure 3.3, was used for this test. Some theoretical equations can be derived to describe the calculation for *MRR*:

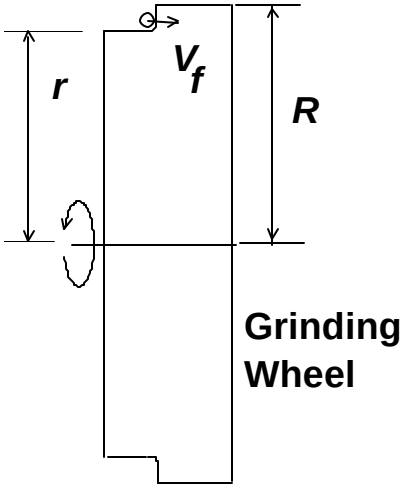

Figure 3.3: Truing profile

$$MRR = p(R^2 - r^2)V_f \qquad (2)$$

where R is the original radius of the grinding wheel, r is the new reduced radius of the grinding wheel after material has been removed, and V_f is the machine cutting speed, or wire feed rate associated with the WEDM machine. Eq. (2) relies on assumptions of constant V_f, and constant r during machining.

Figure 3.4 shows the *MRR* graphs for the two grinding wheels in the study. Diamond grinding wheel I is the Norton Scepter eight inch, 320 grit wheel, and Diamond grinding wheel II is the bronze bond wheel (Inland MD1200N50M-1/4). The figure shows higher *MRR* is possible for the Norton Scepter wheel. This is due to the smaller grit size and material properties of the bronze bonded wheel. The maximum material removal rates of the Norton Scepter wheel and Inland bronze bonded wheel are 27.0 and 23.5 mm^3/min, respectively. The graphs for grinding wheels cannot be compared to the graphs of the other materials due to the difference in performance measured. It should be noted that spark on-

time of 4 µs was not possible with the grinding wheels due to the presence of frequent wire short circuit.

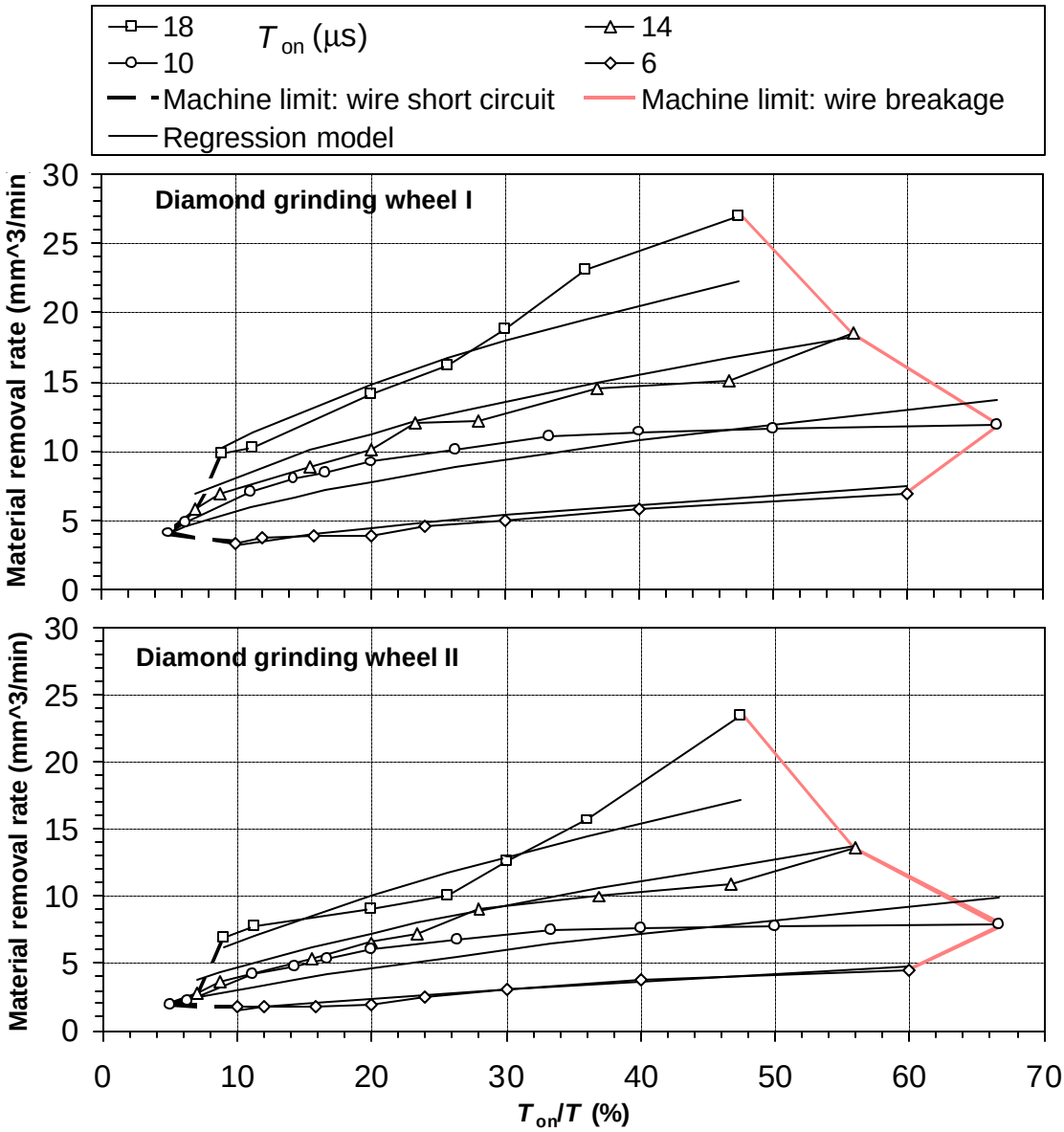

Figure 3.4: Material removal rate graphs for metal bond diamond grinding wheels

3.2.3. Sintered Nd-Fe-B Permanent Magnet

The sintered Nd-Fe-B permanent magnet has the lowest *MRR*, as can be predicted from its material properties. Sintered Nd-Fe-B magnets have density of 7.5 g/cm^3, specific heat of 420 J/kg-K, and melting temperature of 1620 K. As shown in Figure 3.5, the maximum cutting speed possible on a 25.0 mm thick sample is 2.0 mm/min. As with the grinding wheels, using spark on-time of 4 μs is not possible with this material. Energy density delivered with this setting is not adequate to avoid wire short circuit.

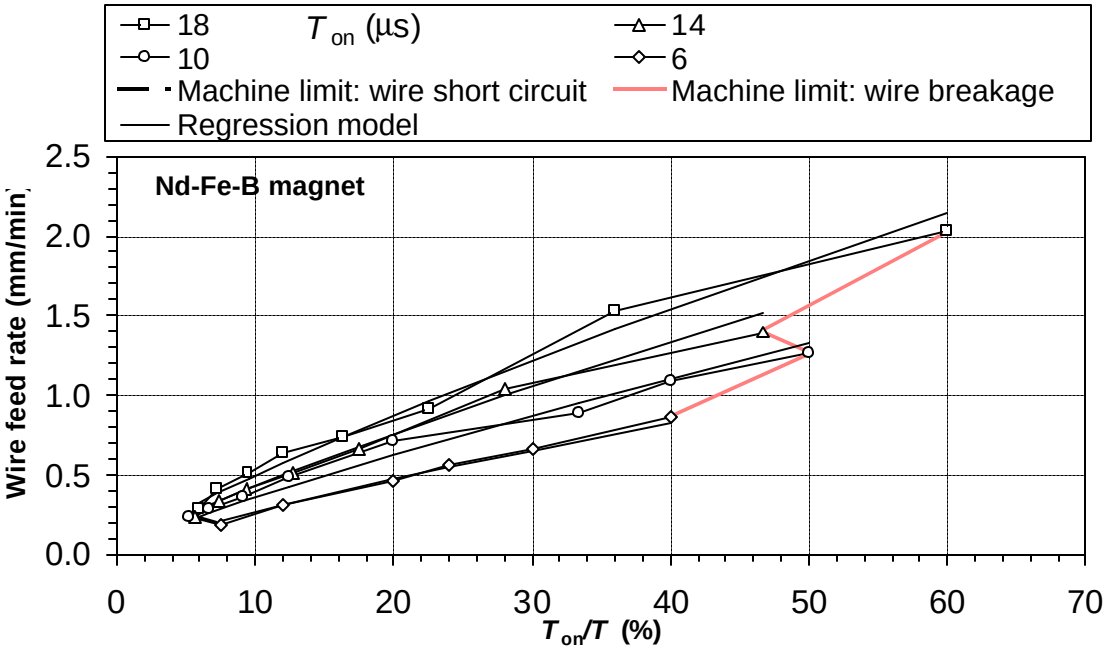

Figure 3.5: Material removal rate graph for sintered Nd-Fe-B magnet

3.2.4. Carbon-Carbon Bipolar Plate

Figure 3.6 shows the *MRR* graph for cutting the carbon-carbon bipolar plate. This material is the easiest to cut by WEDM. The maximum cutting speed achieved during cutting of the carbon-carbon bipolar plate is 304.8 mm/min, the maximum cutting speed of the Brother HS-5100 WEDM machine. This cutting speed is reached by all but one of the spark on-time settings. This limit greatly affects the envelope of process parameters for the carbon-carbon plate. If the WEDM machine did not possess a maximum cutting speed, the shape of the envelope in Figure 3.6 would most likely resemble that of the other figures of *MRR*. The machine limit of wire short circuit is replaced in this figure by the machine limit of spark cycle, *T*. Regression modeling is not feasible due to the complexity of the data. Letters in the graph again signify process parameters to be investigated by SEM in Chapter 4.

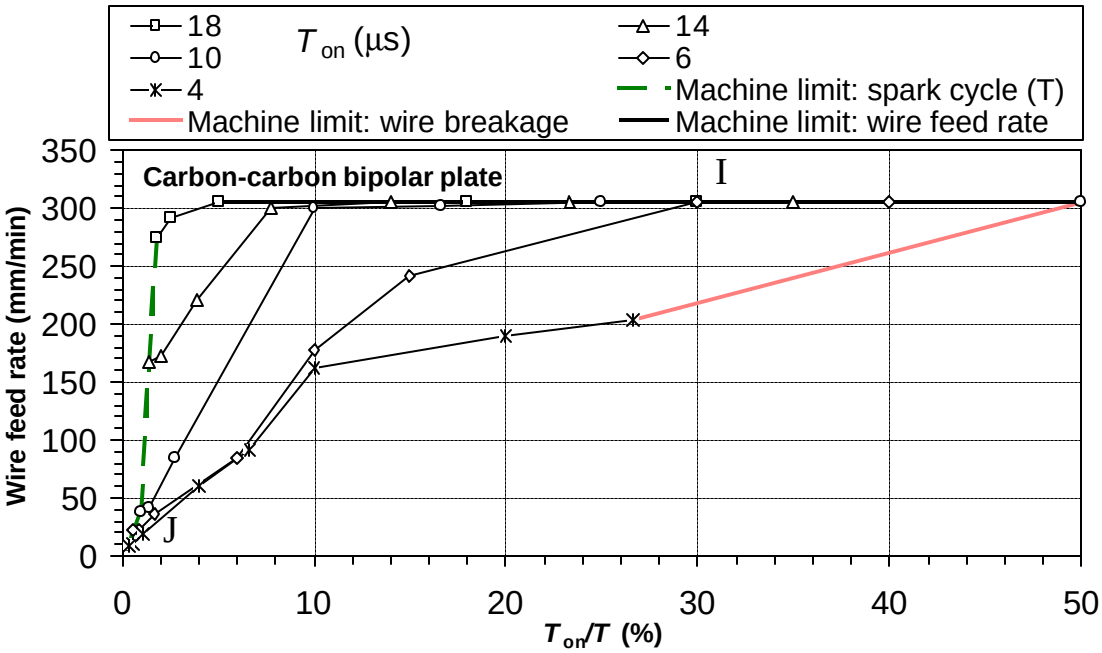

Figure 3.6: Material removal rate graph for carbon-carbon bipolar plate

Cutting the carbon-carbon bipolar plate generates an entirely new set of machine limits not encountered in WEDM of traditional materials. This is due to the fact that cutting this material is much easier and faster than cutting an average workpiece material. As mentioned earlier, the WEDM machine has a limit of 1000 μs for spark cycle, *T*. This is the maximum *T* at which the machine will operate. During cutting the carbon-carbon bipolar plate, the energy density never falls low enough to cause wire short circuit in the allowable *T* range. On the *MRR* graph for the carbon-carbon bipolar plate, the machine limit for wire short circuit is replaced by the on-time ratio associated with the maximum *T*. Another limitation of the machine is the maximum cutting speed, 304.8 mm/min. This limit is easily reached while cutting the carbon-carbon bipolar plate, which is represented by the solid line in the graph on the top of the envelope of feasible process parameters.

3.2.5. Results of Regression Modeling

Table 3.1 shows the results of the regression modeling for every material analyzed. The form of the equation is: $MRR = a \cdot \left(\frac{T_{on}}{T} \right)^{b} \cdot (T)^{c}$. The purpose of regression modeling is to find a mathematical model relating *MRR* to spark cycle (*T*) and percentage on-time (T_{on}/T). Significance of the parameter to the *MRR* increases with increasing size of the value of the

Table 3.1: Results of regression modeling

Type of machining	Material	a(x10^{-3})	b	c	b/c	b/c % difference
Porous metal foam	Fe-Cr-Al foam	13.1	1.51	0.762	1.98	7.29
	316 stainless steel foam	1.90	1.90	1.02	1.86	
Solid material	Carbon steel plate	2.11	1.97	0.718	2.74	11.6
	Nd-Fe-B magnet	1.10	1.38	0.565	2.44	
Rotary	Grinding wheel 1	0.984	1.56	1.10	1.42	3.46
	Grinding wheel 2	0.0910	1.92	1.30	1.48	

parameter's exponential variable.

In all types of machining b is larger than c, suggesting T_{on}/T is the more significant parameter of the two. A ratio of the exponential variable for T_{on}/T to the exponential variable for T has been included in Table 3.1 for each material. This ratio can be considered a measure of the relative importance of the exponential variables. For porous metal foams, solid materials, and rotary machining, the ratios are 1.99 and 1.85, 2.74 and 2.44, and 1.42 and 1.47, which give a percentage difference of 7.29, 11.6, and 3.46%, respectively. The equation for percentage difference of two values consists of the difference of the values divided by their average. This trend of b/c ratio suggests that for a certain type of machining application, this ratio, and this relationship between process parameters will fall within a certain range.

3.2.6. General Results of Material Removal Rate Study

This study developed an envelope of feasible T_{on} and T_{on}/T process parameters to characterize the WEDM process for new advanced engineering materials. A few trends were observed during the study. Material removal rate depends on T_{on} and T_{on}/T in the following respects. Higher T_{on} results in higher material removal rate. The material removal rate increases with increasing T_{on}/T, until the wire breaks due to too much energy density. The material removal rate decreases with decreasing T_{on}/T, until the wire touches the workpiece and causes wire short circuit due to too little energy density. Regression modeling creates a good relationship of material removal rate to the process parameters of T and T_{on}/T for the materials studied.

3.3. Application of Cutting Thin Sections

The envelope of feasible process parameters for the carbon-carbon bipolar plate is applied to select proper process parameters for cutting sections of this material of minimum possible thickness. Amount of energy density applied by WEDM, determined by chosen process parameters at points I and J in Figure 3.6, has an effect on possible minimum thickness of features. Tests were conducted on sintered Nd-Fe-B to investigate this effect. The following sections present application and explanation of results of cutting thin sections.

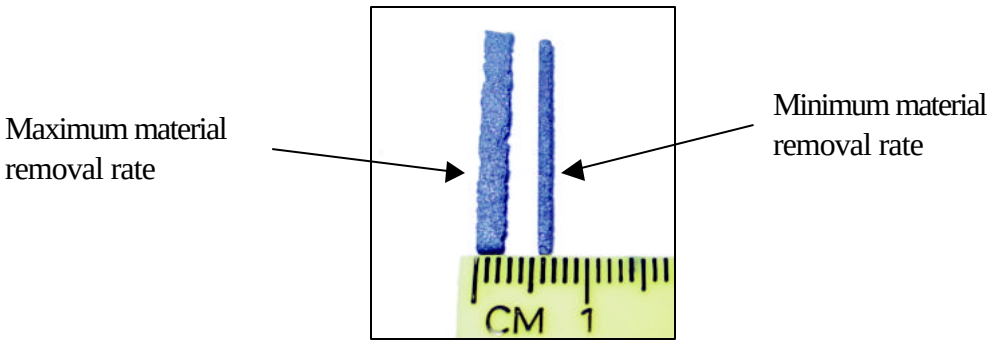

Figure 3.7: Thin sections of carbon-carbon bipolar plate

3.3.1. Thin Section Cutting Application of Carbon-Carbon Bipolar Plate

An application of a feasible envelope of process parameters for a given material regards cutting miniature features. Figure 3.7 shows thin sections of carbon-carbon bipolar plate. The section on the left side of the figure is the cut section corresponding to maximum energy density, point I on the *MRR* graph, and the cut section on the right side corresponds to minimum energy density, point J on the *MRR* graph, with respective thickness dimensions of 2.75 and 1.25 mm. Point a on the graph represents spark on-time, T_{on}, of 18 µs and percentage on-time, T_{on}/T %, of 30.0 %. Point b on the graph represents T_{on} of 4 µs and T_{on}/T % of 0.40 %. Rougher surface characteristics of the section cut with maximum energy

density can be noticed in Figure 3.7. It is clearly noticeable that EDM process parameters have an effect on minimum possible thickness.

3.3.2. Cutting Thin Sections of Sintered Nd-Fe-B Magnet

As noted above, EDM process parameters have a significant effect on possible minimum thickness of a workpiece. One purpose of cutting thin sections of sintered Nd-Fe-B magnet is to generate a model for this effect. EDM uses electrical sparks to generate energy to melt and remove material. The very nature of the EDM voltage cycle, as illustrated in Figure 2.1, suggests energy variation throughout the process. This energy variation, E_v, which is based on the average energy, E_A, required for cutting, is one factor that decides the minimum thickness possible for a workpiece material. Figure 3.8 shows thin sections for three spark on-time, T_{on}, settings, 2, 10, and 18 µs, left to right, respectively, with respective T_{on}/T settings of 2.5, 8.3, and 12 %. The variation of minimum thickness of thin sections, due to variation of cutting energy delivered, is used to approximate relative E_v corresponding to E_A.

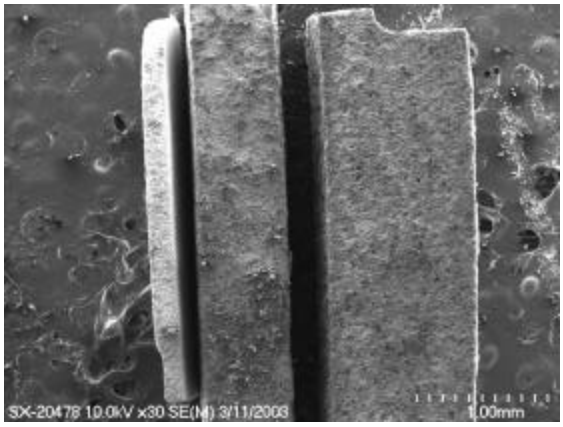

Figure 3.8: Nd-Fe-B magnet thin sections

The determination of E_A is based on the equation for change in energy required to melt workpiece material:

$$E = m \cdot C_p \cdot \Delta T = r \cdot V \cdot C_p \cdot \Delta T \qquad (3)$$

In this equation m, C_p, $?T$, $?$, and V are mass, specific heat, change in temperature, density, and volume of removed material, respectively. The density and specific heat for sintered Nd-Fe-B magnet material are $7.5x10^{-6}$ kg/mm^3 and 420 J/kg-K, respectively. Volume of removed material can be defined by the dimensions of height of workpiece material, length of cut, and width of wire plus gap of removed material on each side of the wire, which is 1.5 x 3.0 x 0.33 mm corresponding to a volume of 1.49 mm^3. Change in temperature is the difference in room temperature and melting temperature. The melting temperature for sintered Nd-Fe-B magnet material is 1620 K. With this information E_A can be found:

$$E_A = \frac{E \cdot V_f}{l_{cut}} \tag{4}$$

In this equation V_f refers to cutting speed and l_{cut} refers to length of cut. V_f depends on EDM process parameters, and is recorded during cutting. Finally, the E_v approximation relies on the assumption that minimum thickness is directly related to E_v. The approximation begins with a hypothesis of E_{v2} based on E_A:

$$\frac{E_{V18}}{thickness_{18}} = \frac{E_{V10}}{thickness_{10}} = \frac{E_{V2}}{thickness_{2}} \tag{5}$$

The subscript in each term refers to the EDM spark on-time (18, 10, and 2 μs) that characterizes the energy setting of the machine.

Table 3.2 summarizes the results obtained in this study. It includes wire cutting speed, E_A, minimum thickness of thin section, and E_v for each spark on-time setting.

Table 3.2: Results of model of cutting thin sections

Spark on-time (μs)	V_f (mm/min)	E_A (J/min)	Thickness (mm)	E_v (J/min)
18	7.62	15.7	1.1	0.825
10	3.81	7.88	0.75	0.563
2	0.229	0.473	0.2	0.150

Figure 3.9 shows a graphical illustration of power in units of J/min vs T_{on} in units of μs. The figure includes data of E_A and E_v from the table for each T_{on} setting.

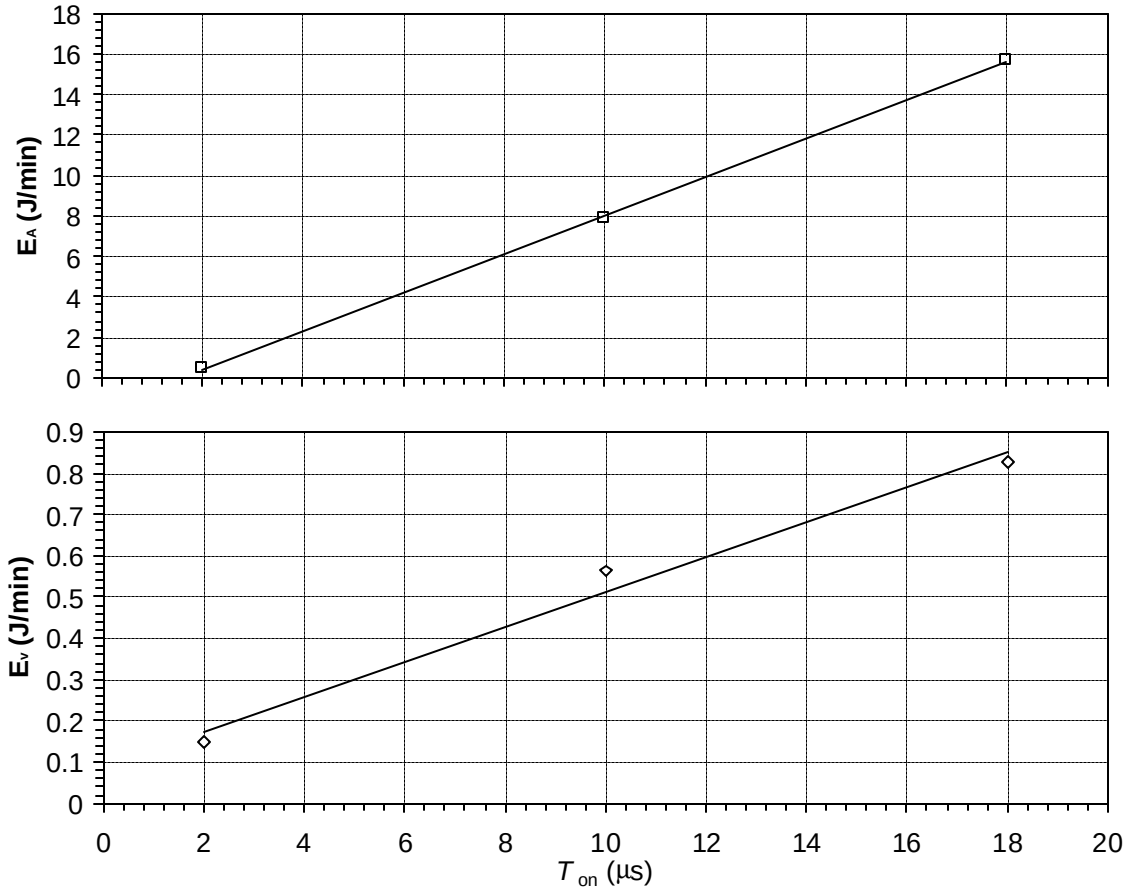

Figure 3.9: Energy graph of E_A and E_v for three T_{on} settings

Chapter 4. Scanning Electron Microscope (SEM) Investigation

Zworykin et al. described the first SEM used to examine the surface of a solid specimen in 1942, working in the RCA Laboratories in the United States. The electron optics of the instrument consisted of three electrostatic lenses with scan coils placed between the second and third lenses [Breton, 2001]. The electron gun was located at the bottom, so the specimen chamber was at a comfortable height for the operator [Breton, 2001]. Since then, the electron microscope has become an important tool for investigating microscopic features. Unlike the optical microscope, which uses a beam of light that is reflected by the surface, SEM uses a beam of electrons that are both absorbed and reflected by the surface. The advantage of SEM includes both a high level of magnification and a large depth of field. The microscope used in this study is the Hitachi S-4700 Field Emission SEM, as shown in Figure 4.1.

Figure 4.1: Hitachi S-4700 field emission SEM [Hitachi, 2003]

One major goal of this study is to perform a qualitative analysis of effects of WEDM process parameters on surface finish. It is thought that machining with increased spark energy, T_{on}, causes rougher surface finish. To investigate this hypothesis, SEM is used to examine samples of porous metal foams and thin sections of Nd-Fe-B magnet that were cut at different WEDM settings.

The materials looked at by SEM are 1. porous metal foams, 2. carbon-carbon bipolar plate, and 3. sintered Nd-Fe-B magnet. The following sections present the results of the SEM analysis of these materials. In the final section is a review of Chapter 4.

4.1. SEM of WEDM Surface of Porous Metal Foams

Samples of two porous metal foam materials, 316 stainless steel and Fe-Cr-Al alloy, were prepared for SEM study. The process parameters of these sections were determined from the four corners of the envelope of process parameters for each material, marked as A, B, C, D, E, F, G, and H in Figure 3.2. In each SEM figure of metal foam the top and bottom picture have magnifications of 500X and 1500X, respectively.

SEM pictures of 316 stainless steel foam are shown in Figure 4.2 and Figure 4.4. Parts (a), (b), (c), and (d) of Figure 4.4 correlate to surface finish due to process parameter settings of the four corners of the material removal rate graph for 316 stainless steel foam. Difference in surface finish due to different spark on-time settings, T_{on}, can be observed from the graphs. Figure 4.4(a) and (b) correspond to T_{on} of 18 μs, and Figure 4.4(c) and (d) correspond to T_{on} of 4 μs.

SEM pictures of Fe-Cr-Al foam are shown in Figure 4.3 and Figure 4.5. Parts (a), (b), (c), and (d) of Figure 4.5 correlate to surface finish due to process parameter settings of

the four corners of the material removal rate graph for Fe-Cr-Al foam. Difference in surface finish due to varying T_{on} is not as evident for the Fe-Cr-Al foam as the 316 stainless steel foam. Figure 4.5(a) and (b) correspond to T_{on} of 18 μs, and Figure 4.5(c) and (d) correspond to T_{on} of 4 μs.

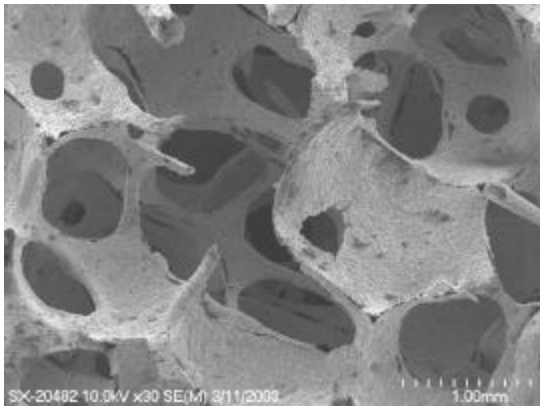

Figure 4.2: 316 stainless steel foam

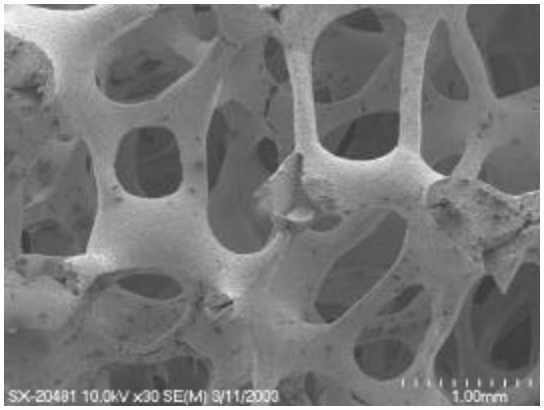

Figure 4.3: Fe-Cr-Al foam

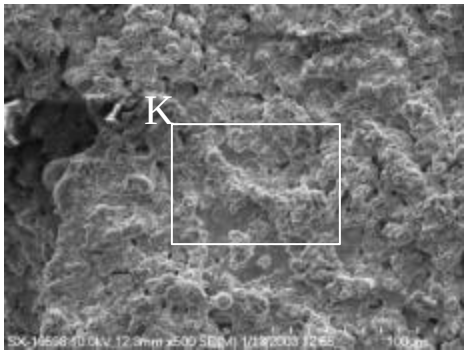

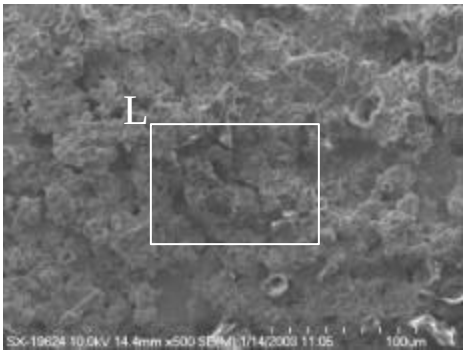

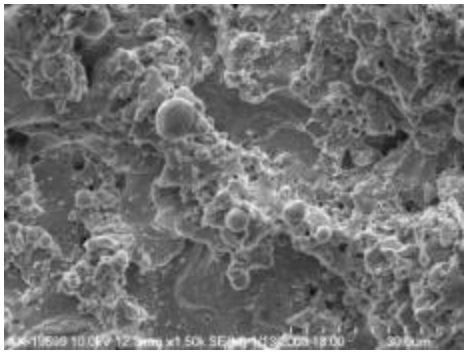

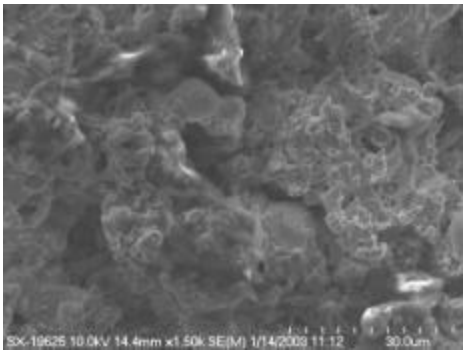

Close-up of K

(a) T_{on} = 18 µs, T_{on}/T = 32.0 % (Point A)

Close-up of L

(b) T_{on} = 18 µs, T_{on}/T = 5.3 % (Point B)

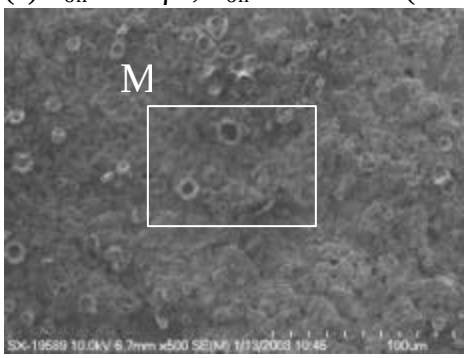

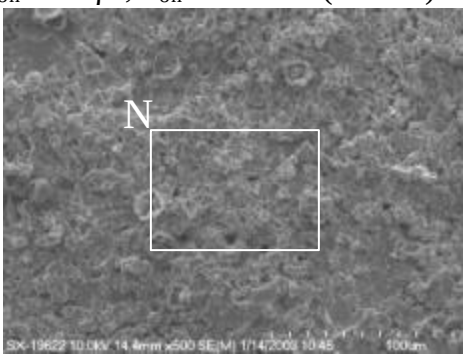

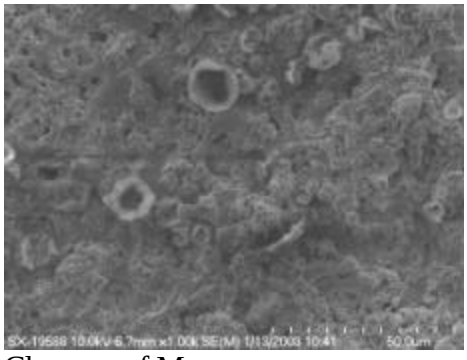

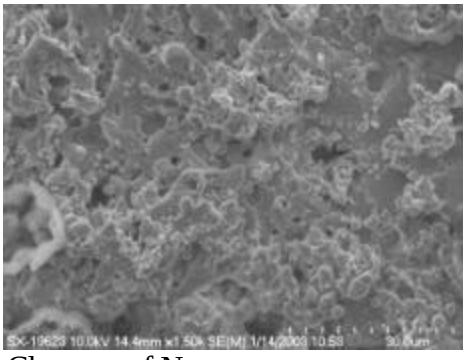

Close-up of M

(c) T_{on} = 4 µs, T_{on}/T = 26.7 % (Point C)

Close-up of N

(d) T_{on} = 4 µs, T_{on}/T = 5.0 % (Point D)

Figure 4.4: SEM micrograph of WEDM of 316 stainless steel foam

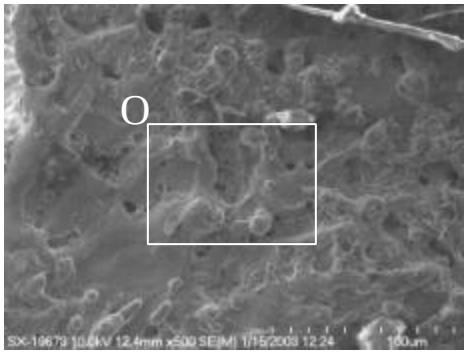

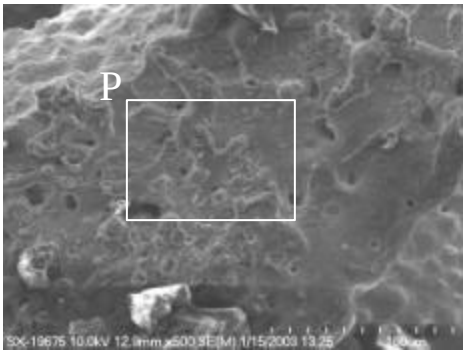

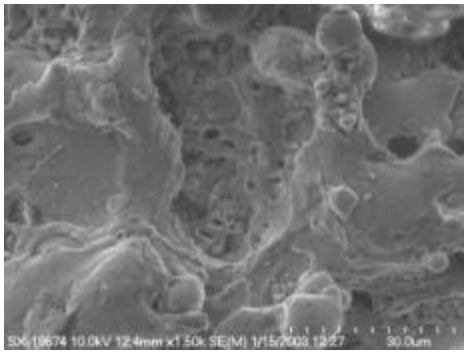

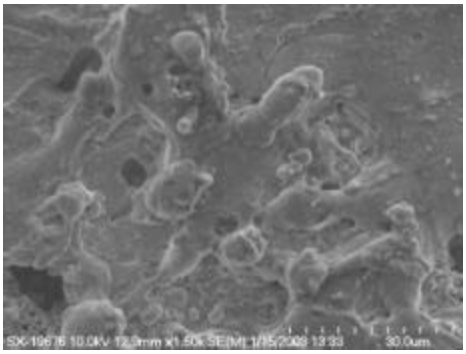

Close-up of O

(a) T_{on} = 18 µs, T_{on}/T = 36.0 % (Point E)

Close-up of P

(b) T_{on} = 18 µs, T_{on}/T = 5.1 % (Point F)

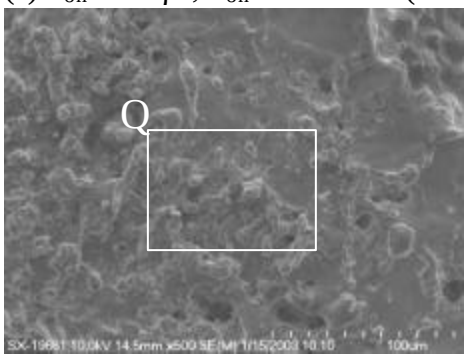

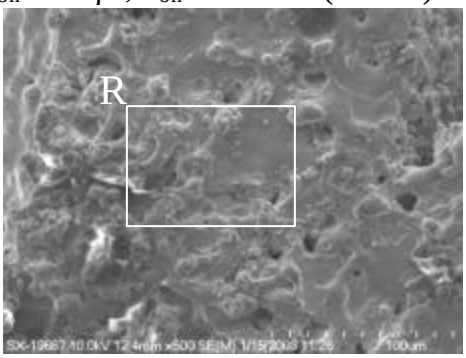

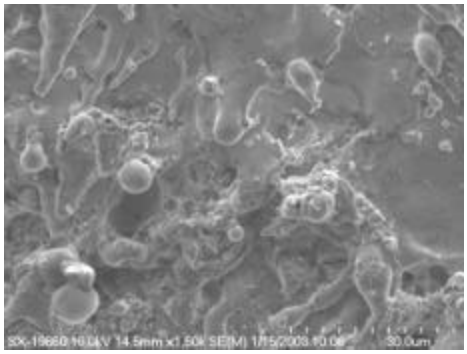

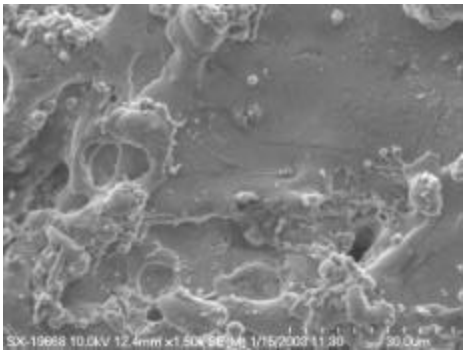

Close-up of Q

(c) T_{on} = 4 µs, T_{on}/T = 26.7 % (Point G)

Close-up of R

(d) T_{on} = 4 µs, T_{on}/T = 4.0 % (Point H)

Figure 4.5: SEM micrograph of WEDM of Fe-Cr-Al foam

4.2. SEM of WEDM Surface of Carbon-Carbon Bipolar Plate

SEM is used to investigate carbon-carbon bipolar plate material cut by the WEDM machine. This is compared to SEM pictures of the carbon-carbon bipolar plate in its original form. Slurry molded carbon fibers, about 0.4 mm long and 0.01 mm in diameter, which are sealed with chemically vapor-infiltrated carbon are also observed.

Figure 4.6 shows SEM pictures of the carbon-carbon bipolar plate. In Figure 4.6(a) and (b) the magnifications from top to bottom are 200, 500, and 1300X. Figure 4.6(a) shows standard carbon-carbon bipolar plate material. Not much can be learned from the first magnification, but as magnification grows so does the detail of pictures. Shapes of carbon fibers become clear as magnification reaches 500X. Carbon fiber surrounded by infiltrated sealing carbon can be seen well as magnification reaches 1300X. Figure 4.6(a) helps to understand the microstructure and slurry-molding process associated with carbon-carbon bipolar plates.

Figure 4.6(b) shows the carbon-carbon bipolar plate that has been machined by WEDM. As can be seen from magnification of 200X, the surface of the machined carbon-carbon bipolar plate is much rougher than that of standard material. Also, the carbon fibers are not as apparent as in Figure 4.6(a). The WEDM machine has melted the carbon fibers and sealing carbon, and recast them together on the surface. In the pictures of magnification 500 and 1300X half hidden shapes of carbon fibers do still seem to be apparent, but not near as prevalent as in Figure 4.6(a).

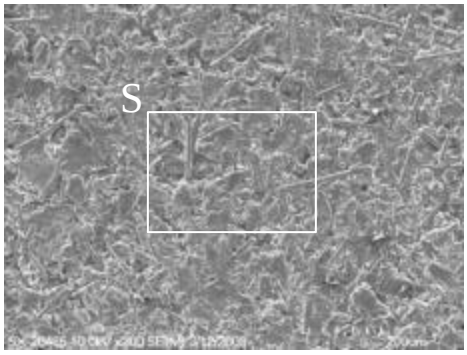

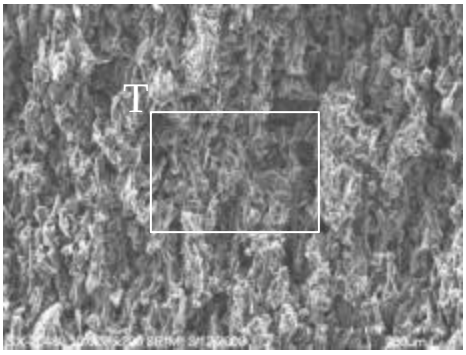

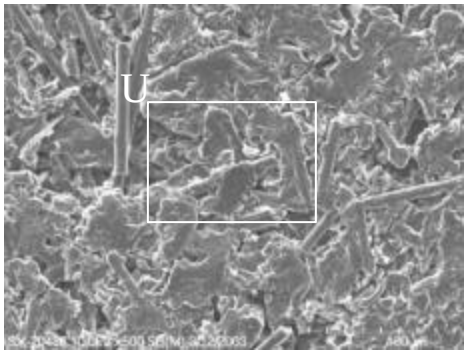

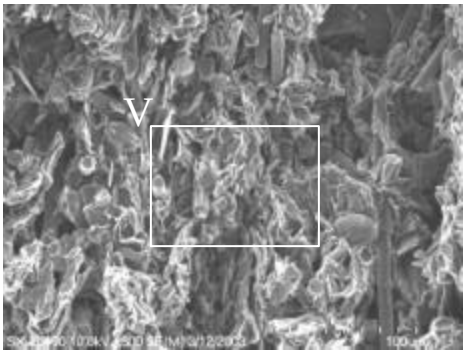

Close-up of S

Close-up of T

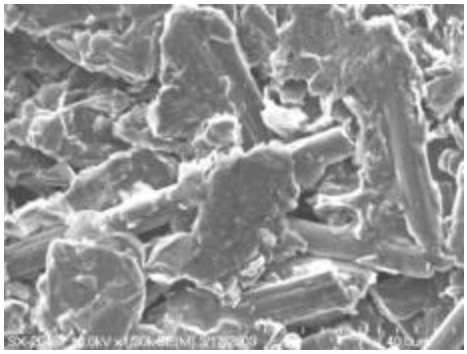

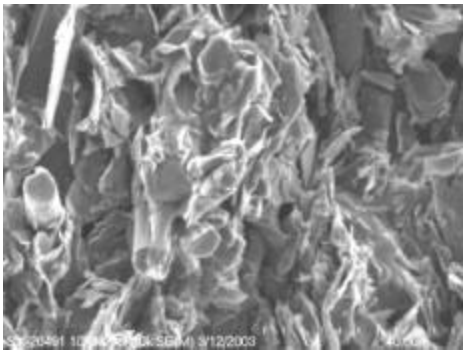

Close-up of U

Close-up of V

(a)

(b)

Figure 4.6: (a) Carbon-carbon bipolar plate (b) Carbon-carbon bipolar plate cut by EDM

4.3. SEM of WEDM Surface of Sintered Nd-Fe-B Magnet Thin Sections

Sections of Nd-Fe-B magnet material were cut to minimum thickness using three different spark on-time, T_{on}, settings, 18, 10, and 2 μs, with 1.5 mm height and 3.0 mm length. SEM is used to compare and contrast surface finish characteristics of these sections.

Figure 4.7(a), (b), and (c) shows surface finish of sintered Nd-Fe-B magnet for three different spark on-time settings, T_{on}, 18, 10, and 2 μs, respectively. It should be noted T_{on} of 2 μs is a special low energy setting not typically used in WEDM. In the figure magnification of pictures from top to bottom is 400, 700, and 1500X. Difference in surface finish between T_{on} of 18 and 10 μs does not appear to be significant, but surface finish of T_{on} of 2 μs does appear to differ from the other two T_{on} settings. In the pictures of the lowest T_{on} setting are more flat regions in between bumps, and the recast layer does not build up as it does in the other pictures. Also, in the picture of 1500X for the lowest T_{on} setting presence of micro-cracks can be seen.

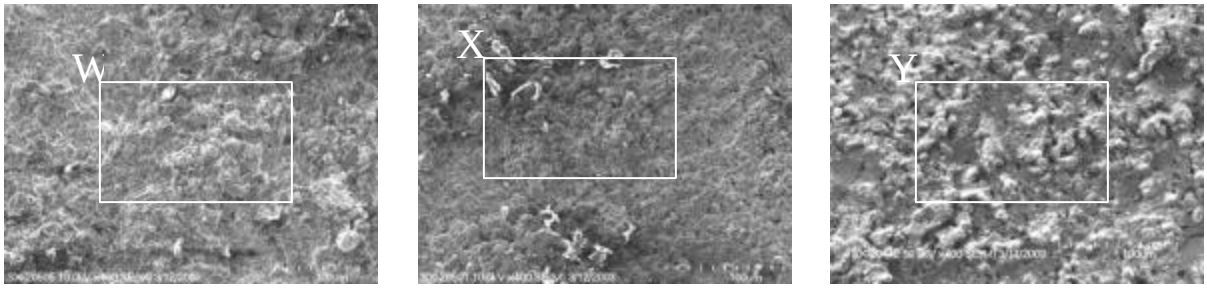

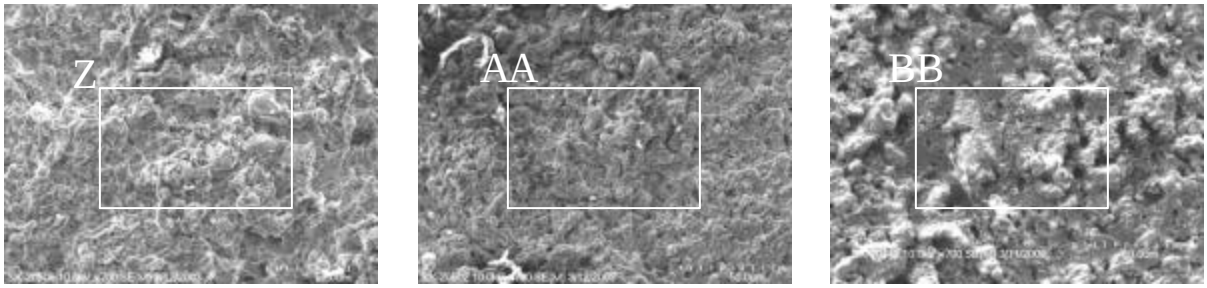

Close-up of W | Close-up of X | Close-up of Y

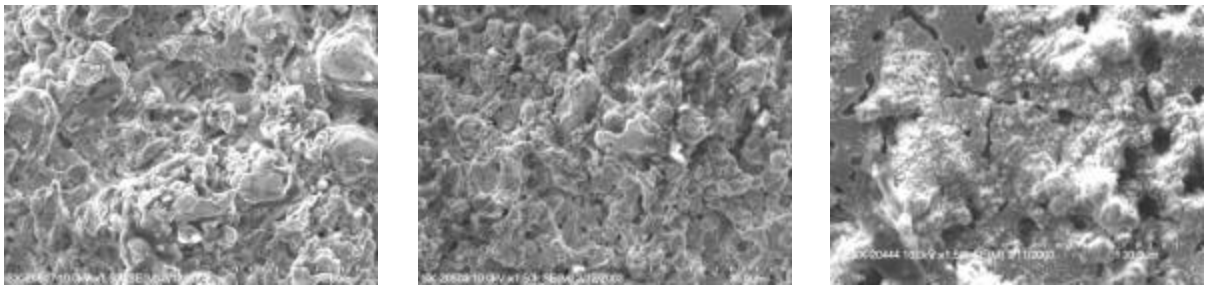

Close-up of Z | Close-up of AA | Close-up of BB

(a) (b) (c)

Figure 4.7: Sintered Nd-Fe-B magnet, (a) 18 ms (b) 10ms (c) 2 ms

Chapter 5. EDM Temperature Measurement Using Infrared Spectrometry

Wire EDM relies on the heat generated from electrical sparks to melt and remove the work-material. This process requires temperature above the melting temperature of the workpiece. The goal of this study is to measure EDM temperature using infrared spectrometry.

Research has been conducted on temperature of the plasma used in EDM. Temperature was determined from measurements of relative intensities of the 411.85 and 413.29 nm Fe I spectral lines. The measured plasma temperature range was from 8000 to 10000 K [Albinski et al., 1996]. Other research has been conducted to measure the wire electrode temperature. The measured wire temperature ranges up to 180^{o}C depending on the cutting conditions [Takeshita, 1997].

Visible light emission of spark and arc can be observed during the EDM spark erosion. This indicates the possibility to use light emission to measure the flash temperature in EDM spark erosion. The electrode and workpiece during EDM are usually submerged in dielectric fluid. Either the water- or oil-based dielectric fluid will block the light emission in the infrared wavelength region. To overcome this problem, the cylindrical wire EDM process [Qu et al., 2002a, 2002b; Rhoney et al., 2002] is used. A spindle drives the workpiece in cylindrical wire EDM. The light emission can be captured by an infrared sensor and used to measure temperature.

The following sections in Chapter 5 gives the experimental setup and presents the results of this study.

5.1. Setup of Spark Temperature Measurement

Three types of workpiece, 1. diamond grinding wheel, 2. copper, and 3. WC-Co, are used in the EDM temperature measurement.

5.1.1. Workpiece Preparation

The preparation of the workpiece is similar to that of the diamond grinding wheel during the material removal rate study. The wheel and hub assembly is mounted to the spindle, which is mounted to the worktable inside the EDM machine, which serves as an electrical ground. The copper and tungsten carbide materials are mounted to the worktable in a different spindle than the diamond grinding wheel. In order to determine the beginning position of the cut, an edge find process was executed. The wire moves toward the workpiece slowly until it is barely touching the workpiece. The wire is then moved a predetermined distance from the workpiece to allow for automatic wire rethreading in the event of wire breakage. During cylindrical wire EDM machining the workpiece does not need to be submerged, only a jet of dielectric fluid is required for flushing. The reason is the wire is only removing material on the surface, and the wire is not embedded within the workpiece material.

However, one major difference is needed for temperature measurements. As mentioned earlier, the dielectric fluid blocks the light emission in the infrared wavelength region. Therefore, the flushing jets must be closed to allow as much light as possible to flow from the EDM process. This is required in order for the spectrometer to receive the signal. But, closed flushing jets hinder the flushing condition of debris and increase the chance of

wire breakage. So the feed rate must be reduced to allow smooth wire EDM operation without wire breakage.

5.1.2. Temperature Measurement Procedure

The spectrometer used was an Ocean Optics USB2000 near-infrared spectrometer. Its wavelength range includes 0.717 to 0.980 μm. This spectrometer uses charge-coupled discharge (CCD) arrays to allow acquisition of an entire spectrum over one sampling time. It is also easily incorporated with Ocean Optic's spectrometer operating data acquisition software, as Figure 5.1(a) shows. Light is collected by an optical fiber and transmitted to the spectrometer for the measurement. The actual signal acquisition, including the grinding wheel, optical fiber, and spark are shown in Figure 5.1(b). The spark is continuous, so the measurement time window is unlimited. A close-up view of the wire, grinding wheel, and optical fiber tip are shown in Figure 5.1(c).

Before temperature measurements are taken, the spectrometer must be calibrated to a known temperature source. Calibration sets each pixel in the spectrometer's CCD array to the appropriate gain [Curry et al., 2003]. This ensures relative irradiance of wavelength, and therefore, blackbody curves and temperatures are correct. The known temperature source used was an Ocean Optics LS-1 tungsten halogen lamp at 3100 K. Temperature measurements with infrared spectrometry must be analyzed with the help of simulation.

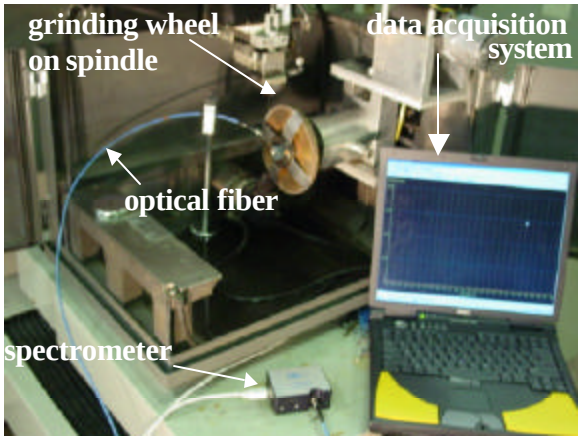

(a)

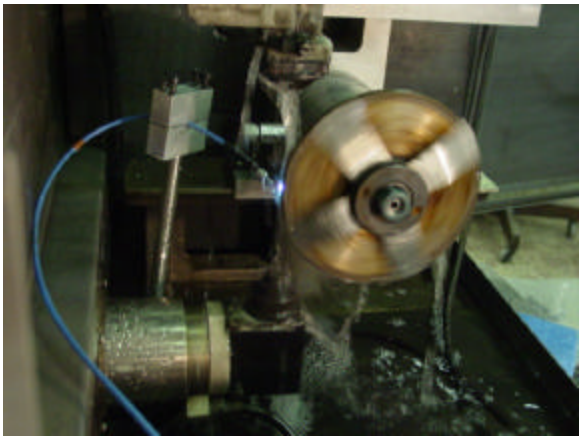

(b)

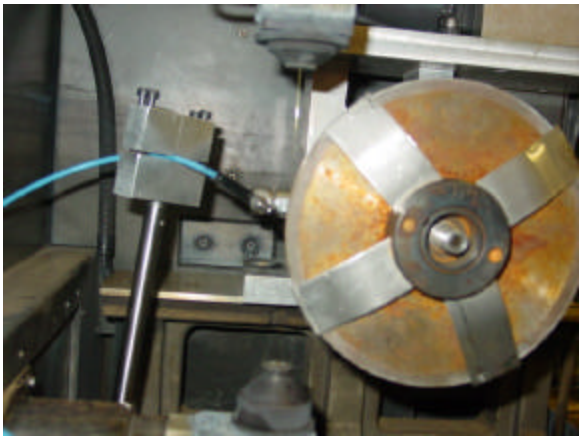

(c)

Figure 5.1: (a) Setup (b) Signal acquisition (c) Close-up view

5.2. Data Analysis and Results

Multiple wavelength techniques use relative intensities of different wavelengths to determine a graybody curve and source temperature. For the method of this study the determination is based on matching the scaled spectrometer output, $R(\lambda)$, to blackbody curves, $E_B(\lambda,T)$, over the wavelength range measured by the spectrometer [Curry et al., 2003].

The equation used for the data analysis method is derived from the blackbody radiation equation,

$$E_B(l,T) = \frac{C_1}{l^5\left(e^{\frac{C_2}{lT}} - 1\right)} \tag{1}$$

$C_1 = 8\pi hc = 4.992 \times 10^{-24}$ Nm^2 and $C_2 = hc/k = 14390$ μmK where h, k, and c are Planck's constant, Boltzmann's constant and the velocity of light, respectively. For radiation at temperature T from a source of emissivity ε passing through a material with transmissivity τ into a spectrometer with an aperture constant α, the spectrometer output function R(λ) is the graybody spectrum

$$R(l) = \frac{a\,e\,t C_1}{l^5\left(e^{\frac{C_2}{lT}} - 1\right)} \tag{2}$$

Assuming that the constants ε, τ, and α are independent of wavelength over the measurement range, a scaled spectrometer output function based on Eq. (2) is written as

$$SR(l) = E(l,T) = \frac{1}{l^5\left(e^{\frac{C_2}{lT}} - 1\right)} \tag{3}$$

S is the adjustable scaling factor accounting for the unknown constants. For source temperatures less than about 3000 K and wavelengths less than 1 μm, the following approximation is valid since the term $\exp(-C_2/\lambda T) << 1$.

$$SR(l) = E(l,T) = \frac{e^{-\frac{C_2}{lT}}}{l^5\left(1-e^{-\frac{C_2}{lT}}\right)} \cong \frac{e^{-\frac{C_2}{lT}}}{l^5} \tag{4}$$

Taking natural logarithm of both sides of Eq. (4) and rearranging gives:

$$\ln\left(\frac{1}{l^5 R(l)}\right) = \frac{C_2}{T}\frac{1}{l} + \ln S \tag{5}$$

Data analysis in this study is based on equation (5). For a given spectrometer measurement, a plot of $\ln(1/\lambda^5 R)$ vs. $1/\lambda$ should be a straight line. Using a linear fit over the wavelength measurement range dictated by the spectrometer, 0.72 μm $\leq \lambda \leq$ 0.92 μm, the temperature T and scale factor S can be obtained from the slope and intercept, respectively.

Figures 5.2-4 show the near infrared spectrometer data taken for wire EDM temperature measurement of copper, WC-Co, and diamond grinding wheel, respectively. The top graph in each figure is the spectrometer output function, $R(\lambda)$ over the wavelength range. The bottom graph in each figure shows the data according to equation (5) with the linear fit. The Y-axis in each bottom graph is $\ln(1/\lambda^5 R)$, and the X-axis is $1/\lambda$ in units of 1/μm. Three temperature measurements were taken for each material. However, the appearance of all temperature measurement graphs is similar to the representative graphs in the figures.

The diamond grinding wheel used in this study is the Inland bronze bonded wheel. The average of the three temperature measurements taken for this workpiece is 2280 K. All of the temperature measurements produced specific spikes at common wavelengths. However, one major difference was that the spikes for the diamond grinding wheel are much

more pronounced. These spikes are due to effects other than thermal, and in the case of the grinding wheel temperature measurements they may significantly affect the method of calculation for temperature.

Table 5.1 shows a summary of the temperature measurement data taken, including average temperature and standard deviation for each material. It shows the average temperature of the measurements for WC-Co is greatest. This makes sense due to the melting temperatures of 1350, 1870, and 3070 K for copper, cobalt, and tungsten carbide, respectively. An interesting point is that the melting temperature for tungsten carbide is higher than temperatures seen in this investigation. It should be noted that during cutting a chemical reaction of oxidation takes place, which increases the overall temperature of the process.

No major trends for the effect of process parameters on temperature can be identified. The average temperatures of the three materials do not deviate significantly, which cannot be explained. Further research in this area is needed. If the spark temperatures are higher than those assumed for the approximation given in Eq. (4), the method based on Eq. (5) might not be valid. However, the same general method for temperature analysis may be used.

Table 5.1: Temperature measurement data in units of K

Material	measurement 1	measurement 2	measurement 3	avg temp	standard deviation
Diamond grinding wheel	2220	2190	2420	2280	143
WC-Co	2320	2300	2250	2290	38.1
Copper	2240	2360	2160	2250	102

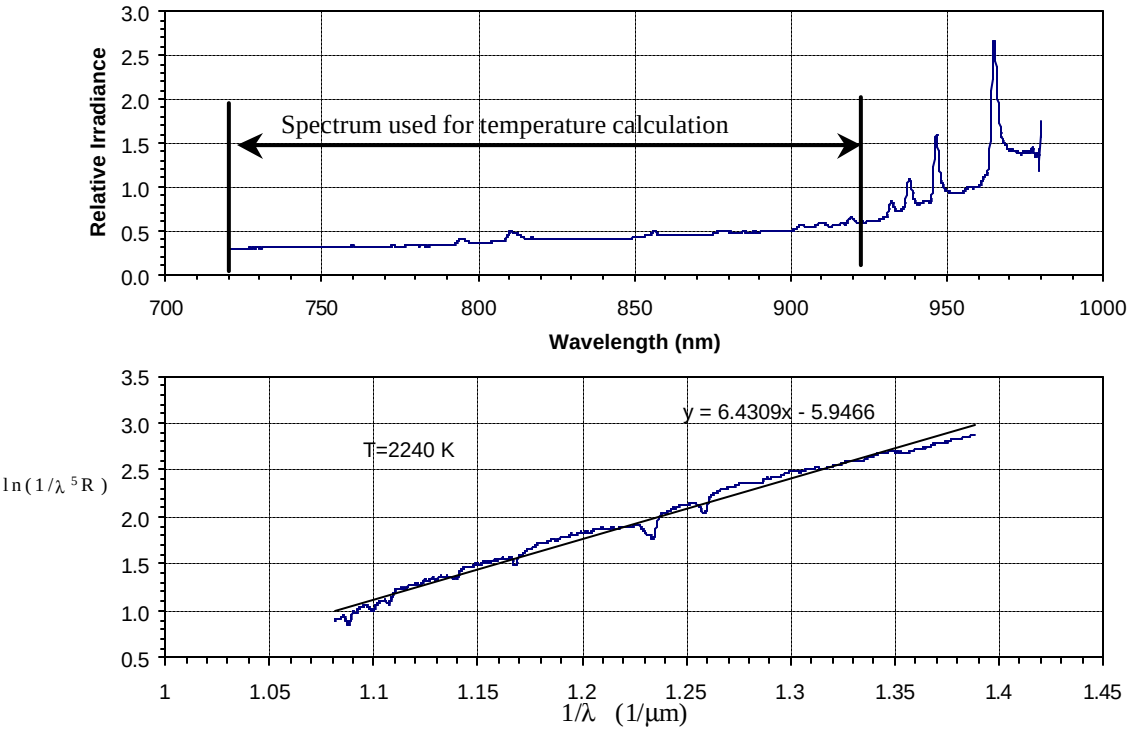

Figure 5.2: Copper temperature measurement 1

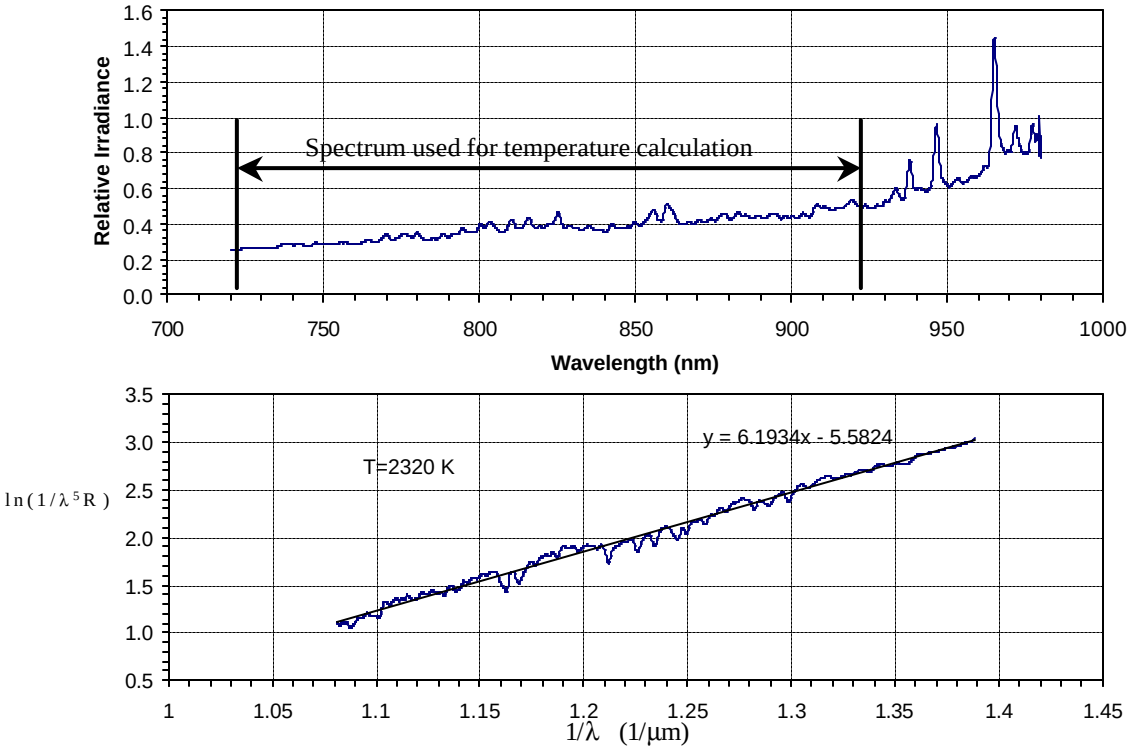

Figure 5.3:WC-Co temperature measurement 1

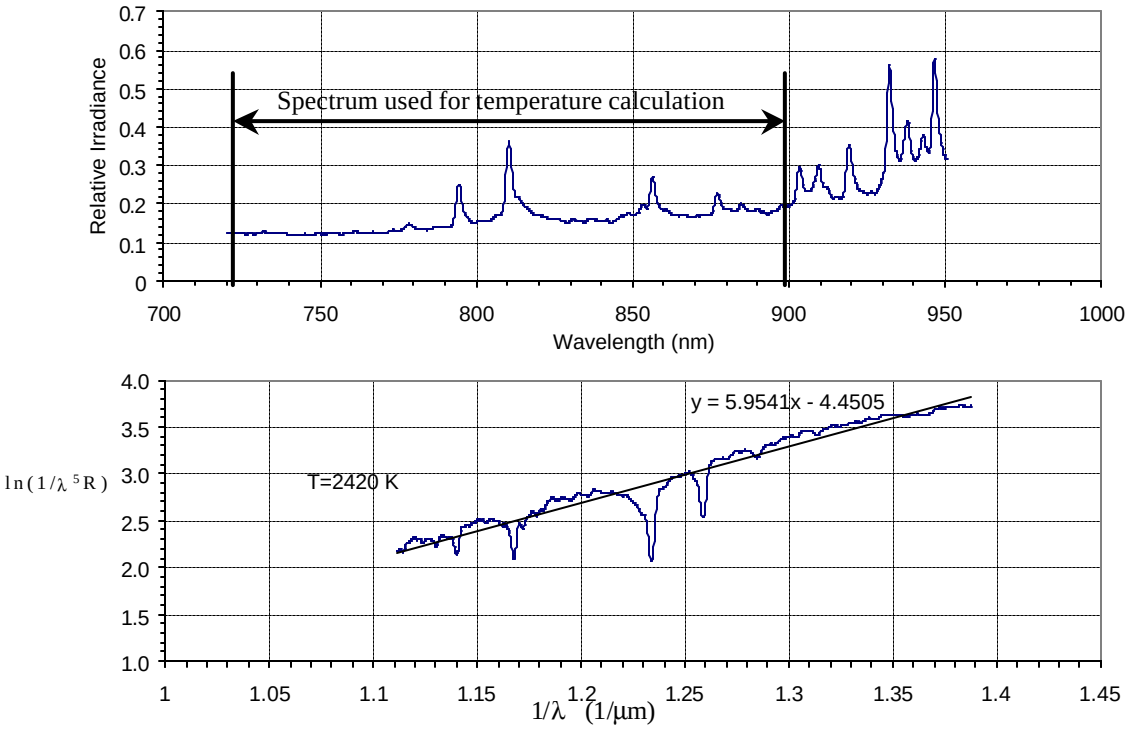

Figure 5.4 Diamond grinding wheel temperature measurement 3

Chapter 6. Conclusions

As the pool of new advanced engineering materials grows, so does the need precise and flexible prototype and low-volume production of components. This has made WEDM an important manufacturing process. Based on this fact, a technical challenge is understanding the limits of WEDM of the new advanced engineering materials. Instead of using mechanical force to remove material, the WEDM process uses the thermal energy or electrical sparks between a thin, traveling wire and the workpiece to melt material.

To begin the research, advanced engineering materials were acquired, including two metal bond diamond grinding wheels, two porous metal foams, a sintered Nd-Fe-B magnet, and a carbon-carbon bipolar plate. The metal bond diamond grinding wheels require cylindrical EDM, as developed by Rhoney et al. [2002].

One goal of this research was to determine the abilities of WEDM of these engineering materials. The *MRR* study investigated the effect of spark on-time duration and spark on-time ratio, two critical WEDM process parameters, on material removal rate. An envelope of feasible process parameters was created for each material. The study also investigated WEDM machine limits including the common limits of wire breakage, wire short circuit, and spark on-time duration. Cutting the carbon-carbon bipolar plate produced some machine limits not encountered in traditional WEDM, due to the ease of cutting this material with the WEDM machine. These include machine limit of maximum speed (304.8mm/min), and machine limit of duration of spark cycle (999 μs). Regression modeling was successfully applied to the *MRR* graphs for each material excluding the carbon-carbon bipolar plate. This is due to the fact that the *MRR* graph of the carbon-carbon bipolar plate is severely affected by the machine limit of maximum cutting speed. A regression model for

this material would not be meaningful. The analysis finds a mathematical model relating the effects of duration of spark cycle and percentage on-time to *MRR*. The regression modeling produced some interesting results. The exponential variables of the process parameters selected, duration of spark cycle and percentage on-time, exhibit a relationship to each other specific to the type of machining application involved; machining of porous metal foam, cylindrical WEDM of diamond grinding wheel, and standard WEDM of a solid workpiece.

The envelope of feasible process parameters was applied to cut carbon-carbon bipolar plate sections of minimum thickness. The corners of the envelope relating to maximum and minimum energy density were used for process parameter selection. The respective minimum thickness values of these energy density settings were 2.75 and 1.25 mm.

It is clear from cutting thin sections of the carbon-carbon bipolar plate that process parameter selection has an effect on possible minimum thickness for a given material. The next step was to investigate this effect. Three spark on-time settings (18, 10, and 2 μs) were used to machine thin sections of sintered Nd-Fe-B magnet material. These settings respectively produced minimum thickness values of 1.1, 0.75, and 0.20 mm. A mathematical model was attempted based on the equation for change in energy required to melt workpiece material. The model includes calculations for average energy of the WEDM process based on cutting speed, as well as calculations for energy variation in the WEDM process based on the minimum thickness values.

SEM investigation was performed on the porous metal foams, carbon-carbon bipolar plate, and sintered Nd-Fe-B magnet thin sections. The main goal of this investigation was to qualitatively characterize surface features of these materials. The study of porous metal

foams and sintered Nd-Fe-B magnet thin sections consisted of noting differences of the surface characteristics due to process parameter selection.

By using SEM a qualitative study of the effect of process parameter selection on surface finish has been performed on porous metal foams. The process parameters selected are the four corners of the envelope of process parameters on the *MRR* graphs for 316 stainless steel foam and Fe-Cr-Al foam. As can be expected, surface finish generally looks rougher as energy density is increased.

The carbon-carbon bipolar plate was also looked at. Carbon fibers in sealing carbon after the slurry molding process and a section of the carbon-carbon bipolar plate machined by WEDM are observed. Differences of the face surface and the surface of material recast by WEDM are noted.

Three thin sections of sintered Nd-Fe-B magnet are also observed in the SEM study. As with the porous metal foams, differences of surface finish due to energy density delivered are observed. SEM investigation of the sintered Nd-Fe-B magnet thin sections shows the major difference is noticed in the section cut with the smallest energy density.

The WEDM process relies on thermal effects to remove material. Temperature measurements were taken during cylindrical WEDM of three materials; 1. metal bond diamond grinding wheels, 2. WC-Co, and 3. copper. The method of temperature measurement was infrared spectrometry over the wavelength range of $0.72\ \mu m \leq \lambda \leq 0.92\ \mu m$. Results of data analysis produced plots of $\ln(1/\lambda^5 R)$ vs. $1/\lambda$, which determined temperature values for each experiment. Some source for error occurred in the experiments due to spikes in relative irradiance over the wavelength range, most notably for the metal bond diamond grinding wheel. These spikes are due to effects other than thermal, and affect

the temperature measurements an unknown amount. It is believed that different materials generate different temperatures in WEDM cutting. This study did not produce temperatures that deviated greatly among the three materials. Further research will be conducted on this subject.

REFERENCES

Albinski, K., Karol, M., Miernikiewicz, A., Stefan, L., and Malota, M. The temperature of a plasma used in electrical discharge machining. Plasma Sources Science Technology. v5, pp. 736-742, 1996.

Ashby, M., Fleck, N.A., Hutchinson, J.W., Gibson, L.J., Wadley, H., Evans, A.G., Wadley, H.N., 2000, Metal Foams - A Design Guide, Butterworth-Heinemann.

Banhart, J. Manufacture, Characterization and Application of Cellular Metals and Metal Foams, Progress in Material Science. v46, pp. 559-632, 2001.

Bessman, T., Klett, J., Henry, J., Lara-Curzio, E. Carbon/Carbon Composite Bipolar Plate for Proton Exchange Membrane Fuel Cells. Journal of The Electrochemical Society. v147 n11, 2000.

Breton, B. The Early History and Development of The Scanning Electron Microscope. Website of Online Information, 2003. http://www2.eng.cam.ac.uk/~bcb/history.html.

Curry, A. C., Shih, A. J., Kong, J. and Scattergood, R. O. Grinding Temperature Measurements in MgO-PSZ Using Infrared Spectrometry. Journal of the American Ceramic Society. 2003.

Hitachi High Technologies America – Electron Microscope Division Website. Website of Online Information, 2003.
http://www.hitachi-hhta.com/elec_micro_div/emfas/emfas_s4700.htm.

Hocheng, H., Lei, W., Hsu, H. Preliminary Study of Material Removal in Electrical-Discharge Machining of SiC/Al. Journal of Materials Processing Technology. v63, pp. 813-818, 1997.

Kozak, J., Rajurkar, K., and Wang, S. Material Removal in WEDM of PCD Blanks. Journal of Engineering for Industry. v116, pp. 363-369, 1994.

Lok, Y., and Lee, T. Processing of Advanced Ceramics Using the Wire-Cut EDM Process. Journal of Materials Processing Technology. v63, pp. 838-843, 1997.

Qu, J., Shih, A. J., and Scattergood, R. O. Development of the Cylindrical Wire Electrical Discharge Machining Process, Part I: Concept, Design, and Material Removal Rate. ASME Journal of Manufacturing Science and Engineering. v124 n3, pp. 702-707, 2002a.

Qu, J., Shih, A. J., and Scattergood, R. O. Development of the Cylindrical Wire Electrical Discharge Machining Process, Part 2: Surface Integrity and Roundness. ASME Journal of Manufacturing Science and Engineering. v124 n4, pp. 708-714, 2002b.

Rajurkar, K. University of Nebraska at Lincoln. Website of Online Information, 2003. http://www.unl.edu/nmrc/Processmech/Processmech.htm.

Rhoney, B. K., Shih, A. J., Scattergood, R. O., Akemon, J. L., Gust, D. J., and Grant M. B. Cylindrical Wire Electrical Discharge Machining of Metal Bond Diamond Wheels for Ceramic Grinding. International Journal of Machine Tool and Manufacture. v42, pp. 1355-1362, 2002.

Suzuki, K., Uematsu, T., and Nakagawa, T. On-Machine Trueing/Dressing of Metal Bond Diamond Grinding Wheels By Electro-Discharge Machining. CIRP-Annals. v36 n1, 1987.

Takeshita, S., and Masanori, K. Measurement of Wire Electrode Temperature in WEDM Process Utilizing Sensitivity Change of the Detection of Discharge Location. Journal of the Japan Society of Precision Engineering. v63 n9, 1997.